# Numerical Modeling of Injection and Mineral Trapping of $CO_2$ with $H_2S$ and $SO_2$ in a Sandstone Formation

*Tianfu Xu[1], John A. Apps[1], Karsten Pruess[1], and Hajime Yamamoto[2]*

[1]Earth Sciences Division, Lawrence Berkeley National Laboratory, University of
   California, Berkeley, CA 94720, USA

[2]Civil Engineering Research Institute, Taisei Corporation, 344-1, Nase-cho, Totsuka-ku,
   Yokohama 245-0051, Japan

**Abstract.** Carbon dioxide ($CO_2$) injection into deep geologic formations could decrease the atmospheric accumulation of this gas from anthropogenic sources. Furthermore, by co-injecting $H_2S$ or $SO_2$, the products respectively of coal gasification or combustion, with captured $CO_2$, problems associated with surface disposal would be mitigated. We developed models that simulate the co-injection of $H_2S$ or $SO_2$ with $CO_2$ into an arkose formation at a depth of about 2 km and 75$^{\circ}$C. The hydrogeology and mineralogy of the injected formation are typical of those encountered in Gulf Coast aquifers of the United States. Six numerical simulations of a simplified 1-D radial region surrounding the injection well were performed. The injection of $CO_2$ alone or co-injection with $SO_2$ or $H_2S$ results in a concentrically zoned distribution of secondary minerals surrounding a leached and acidified region adjacent to the injection well. Co-injection of $SO_2$ with $CO_2$ results in a larger and more strongly acidified zone, and alteration differs substantially from that caused by the co-injection of $H_2S$ or injection of $CO_2$ alone. Precipitation of carbonates occurs within a higher pH (pH > 5) peripheral zone. Significant quantities of $CO_2$ are sequestered by ankerite, dawsonite, and lesser siderite. The $CO_2$ mineral-trapping capacity of the formation can attain 40-50 kg/m$^3$ medium for the selected arkose. In contrast, secondary sulfates precipitate at lower pH (pH < 5) within the acidified zone. Most of the injected $SO_2$ is transformed and immobilized through alunite precipitation with lesser amounts of anhydrite and minor quantities of pyrite. The dissolved $CO_2$ increases with time (enhanced solubility trapping). The mineral alteration induced by injection of $CO_2$ with either $SO_2$ or $H_2S$ leads to corresponding changes in porosity.

Significant increases in porosity occur in the acidified zones where mineral dissolution dominates. With co-injection of $SO_2$, the porosity increases from an initial 0.3 to 0.43 after 100 years. However, within the $CO_2$ mineral-trapping zone, the porosity decreases to about 0.28 for both cases, because of the addition of $CO_2$ mass as secondary carbonates to the rock matrix. Precipitation of sulfates at the acidification front causes porosity to decrease to 0.23. The limited information currently available on the mineralogy of naturally occurring high-pressure $CO_2$ reservoirs is generally consistent with our simulations.

**Key words.** $CO_2$ sequestration, acid gas injection, mineral trapping, numerical simulation, Arkose formation.

## 1. Introduction

Concern over the consequences of global warming due to increasing levels of anthropogenic carbon dioxide ($CO_2$) in the atmosphere has led to a variety of proposals to curtail, if not prevent, further increases. One such approach is to inject $CO_2$ from stationary generators (such as fossil-fuel power plants) into reasonably accessible structural reservoirs in deep permeable geologic formations. Candidates include aquifers in sedimentary formations, structural traps in depleted oil and gas fields, and deep unmineable coal seams. Deep aquifers are relatively abundant in certain regions of the United States, and therefore are logical targets for the eventual disposal of $CO_2$. Such aquifers commonly contain brackish or saline water, and those with salinities exceeding 10,000 mg/L total dissolved solids are excluded by the U.S. Environmental Protection Agency as underground sources of drinking water or USDWs as defined in 40 CFR § 144.3 (U.S. EPA, 2001).

Previous investigations of $CO_2$ disposal in aquifers include geochemical (Gunter, 2000; Perkins et al, 2002; Xu et al., 2004; Zerai, 2006) and hydrologic modeling (Pruess et al., 2003), reactive transport models (Johnson et al., 2001; McPherson and Lichtner, 2001; Knauss et al., 2005; White et al., 2005; Xu et al., 2005), laboratory experiments

(Pearce et al., 1996; Rochelle et al., 1996; Gunter et al., 1997; Soong et al., 2004; Carroll and Knauss, 2005; Kaszuba, et al., 2003 and 2005; Palandri and Kharaka, 2005; Pokrovsky et al., 2005; Rosenbauer et al., 2005), and field studies (Lohuis, 1993; Gunter et al., 1993; Bachu et al., 1994; Perkins and Gunter, 1995; Gunter et al., 1996 and 1997; Kharaka et al., 2006). Large-scale aquifer disposal of $CO_2$ is currently practiced in the Norwegian sector of the North Sea (Korbol and Kaddour, 1995).

Conventional coal-burning power plants are one of the primary contributors of excess $CO_2$ to the atmospheric inventory. However, the energy penalty for separation and compression of $CO_2$ from conventional coal combustion is steep and could lead to a 30 – 40% reduction in useable power output (Nsakala et al., 2001). More technologically advanced integrated gas combined cycle (IGCC) plants, in which coal is gasified with restricted oxygen, are thermodynamically more efficient (i.e., produce less $CO_2$ for a given power output) and are more suitable for $CO_2$ capture. Therefore, if $CO_2$ capture and deep subsurface disposal were to be considered seriously, the preferred approach would be to build replacement IGCC plants with integrated $CO_2$ capture, rather than retrofit existing conventional plants.

The fate of minor quantities of sulfur and nitrogen compounds during combustion or gasification is of considerable interest, as their release into the atmosphere leads to the formation of urban ozone and acid rain, the destruction of stratospheric ozone, and global warming. Coal also contains many trace elements that are potentially hazardous to human health and the environment, such as mercury and arsenic, and their release into the atmosphere is restricted under the Clean Air Act Amendments (CAAA) of 1990. During $CO_2$ separation and capture, these constituents could inadvertently contaminate the separated $CO_2$ and be co-injected. The concentrations and speciation of the co-injected contaminants would differ markedly, depending on whether $CO_2$ is captured during the operation of a conventional power plant or an IGCC plant. The specific nature of the plant design and $CO_2$ separation technology could also afford an opportunity to deliberately capture environmental pollutants in the gaseous state and co-inject them with the $CO_2$ to mitigate problems associated with co-disposal with ash in surface impoundments. With the deliberate and efficient separation and capture of volatile

pollutants, their concentrations would be roughly equivalent to their concentrations in the coal feed.

In this study, we evaluate the co-injection of either sulfur dioxide ($SO_2$) or hydrogen sulfide ($H_2S$) with $CO_2$. $SO_2$ would have to be deliberately removed from the flue gas exhaust using flue gas desulphurization (FGD) technology prior to separation of $CO_2$ using methyl ethanolamine (MEA) absorption/stripping process in conventional plants to prevent poisoning of the MEA. The recovery of $SO_2$ in the FGD circuit would, however, require some modifications in conventional practice. In contrast, $H_2S$ is very conveniently separated together with $CO_2$ using MEA in IGCC plants (Trevino Coca, 2003).

A precedent for the co-injection of $H_2S$ with $CO_2$ already exists, as these acid gases were separated during natural gas production in western Canada and re-injected into deep hydrocarbon reservoirs and saline aquifers (Bachu et al., 2005). By the end of 2002, approximately 40 of such acid-gas injection facilities were active having disposed of close to 1.5 Mt $CO_2$ and 1 Mt $H_2S$. Approximately 16 acid-gas injection facilities are also operating in the United States (Bachu et al., 2005). The relatively trouble-free operation of these facilities suggests that acid-gas injection is a mature and safe technology that can be applied under similar conditions elsewhere. Current acid-gas injection operations would be somewhat analogous to future large-scale co-disposal of $H_2S$ with $CO_2$ from IGCC plants. However, whereas acid gases from natural gas treatment range in composition from 2 to 84 vol. % $H_2S$, most coals contain no more than 5 wt.% sulfur, and therefore the concentration of $H_2S$ in $CO_2$ from IGCC plants is unlikely to exceed 1.5 vol. %.

Knauss et al. (2005) have already presented the results of reactive transport simulations to investigate the impact of mixtures of dissolved $CO_2$, $H_2S$, or $SO_2$ on a geological formation. The results suggest that relatively high concentrations of $H_2S$ in $CO_2$ injection would not adversely impact injectivity compared to the injection of $CO_2$ alone, while co-injection of $SO_2$ may produce anhydrite in quantities sufficient to decrease formation porosity and permeability. A significant conclusion is that, if co-injection can be accomplished, the costs associated with separation and disposal of the gases would be minimized. Knauss et al. (2005) used an analytical expression to calculate

a 1-D radial Darcy flow that approximates the flow field. A single aqueous flow phase was used in which $CO_2$ and other acid gases were dissolved. The simulations extended to only 100 years, whereas the alteration of primary minerals and precipitation of secondary carbonates are expected to take place over much longer time frames. Gunter et al. (2000) used a batch geochemical model to simulate the interaction of industrial waste streams comprising $CO_2$ and $H_2S$ with the minerals in typical carbonate and sandstone aquifers from the Alberta Basin, Canada. The results show that these acid gases can be neutralized with formation of secondary minerals, such as calcite, siderite, anhydrite/gypsum and pyrrhotite. As expected, siliciclastic aquifers demonstrate better "mineral trapping" characteristics for $CO_2$ than carbonate aquifers, because high-pressure $CO_2$ enhances carbonate dissolution, and the availability of co-sequestering hydroxide components such as $Mg(OH)_2$, $Ca(OH)_2$ and $Fe(OH)_2$ are less abundant in carbonates.

Mineral alteration rates due to injection of $CO_2$ in deep aquifers are very slow, especially with respect to aluminosilicates, and extensive alteration is not expected during experimental studies in the laboratory. Experiments simulating the injection horizon environment have been conducted for up to several months in duration, with only minimal alteration and undetectable concentrations of secondary alteration phases. The problem can be circumvented in part through experimental studies at substantially elevated operating temperatures and pressures. Although such studies can provide useful insights, their value is constrained by dissimilarities in system rates, mechanisms, and reaction products. Experimental studies must therefore be supplemented by computer simulations with due consideration to model calibration using, where possible, both laboratory experimental data, and/or field data reflecting evolving or evolved natural systems.

In earlier papers, we performed a series of modeling studies in which various geochemical aspects of $CO_2$ injection were investigated. In Xu et al. (2004), we presented a comparative analysis of the chemical interaction of aqueous solutions under high $CO_2$ partial pressures with three different rock types; (1) glauconitic sandstone from the Alberta Sedimentary Basin, (2) an arenaceous sediment from the Gulf Coast of the United States, and (3) a dunite. Two subsequent studies focused on reactive transport simulations involving only a quartzose lithic arkose representative of the Frio Formation

of the Texas Gulf Coast. The Frio formation is the shallowest of three reservoir quality sandstones and is found at depths ranging between 5,000 and 20,000 ft., sufficient to ensure adequate $CO_2$ densities for effective disposal. The first study involved $CO_2$ injection in a 1-D radial region surrounding the injection well to analyze $CO_2$ immobilization through carbonate precipitation (Xu et al., 2003); the second presented simulation results on mass transfer, mineral alteration, and consequent $CO_2$ sequestration in the same arkose, when confined on either side by a reactive shale (Xu et al., 2005).

In this study, we present numerical simulations of the injection of $CO_2$-$H_2S$ and $CO_2$-$SO_2$ mixtures into an arkose with similar hydrogeologic properties and mineral composition to that used in the preceding two studies.  Our objectives are (1) to analyze changes in aqueous chemical composition, mineral alteration, acid-gas immobilization through precipitation, and changes in porosity induced by the injection, and (2) to compare modeling results with prior investigations and with limited field observations of analogous natural systems as a basis for validation. We use a fully coupled model of multiphase $CO_2$ fluid flow into a saline aqueous ($H_2O$ + NaCl) phase, transport of aqueous species, and geochemical reactions.  Reactive geochemical transport simulations are performed over a period of 10,000 years. The sensitivity of the model to differing dissolution rates and kinetic schemes on the evolution of the chemical system and on $CO_2$ sequestration are also addressed.


## 2. Modeling Approaches


### 2.1. Simulation method

The present simulations employed the nonisothermal reactive geochemical transport code TOUGHREACT (Xu and Pruess, 2001; Xu et al., 2006). This code introduces reactive chemistry into the multiphase fluid and heat flow code TOUGH2 (Pruess, 2004). More information on the TOUGHREACT can be found at the website (http://www-esd.lbl.gov/TOUGHREACT/). A new fluid property module, ECO2N, based on work by Spycher and Pruess (2005) was used, which provides an accurate description of the thermophysical properties of mixtures of water and $CO_2$ under conditions typically encountered in saline aquifers of interest for $CO_2$ disposal ($10\ ^{o}C \le T \le 110\ ^{o}C$; $P \le 600$

bars).

Our modeling of flow and transport in geologic media is based on space discretization by means of integral finite differences (IFD) (Narasimhan and Witherspoon, 1976). The IFD method provides for flexible discretization of geologic media by allowing the use of irregular grids, which is well suited for simulation of flow, transport, and fluid-rock interaction in heterogeneous and fractured rock systems with varying petrology. For regular grids, the IFD method is equivalent to the conventional finite difference method. An implicit time-weighting scheme is used for the individual components of the model, consisting of flow, transport, and kinetic geochemical reactions. TOUGHREACT uses a sequential iteration approach similar to that described by Yeh and Tripathi (1991). After solution of the flow equations, the velocities and saturations of the aqueous phase are used for aqueous chemical transport simulation. Chemical transport is then solved on a component basis. Resulting concentrations obtained from the transport and $CO_2$ gas pressures in the multiphase flow calculation are substituted into the chemical reaction model. The system of chemical reaction equations is solved on a grid-block basis by Newton-Raphson iteration, similar to that used by Parkhurst et al. (1980), Reed (1982), and Wolery (1992).

Changes in porosity and permeability due to mineral dissolution and precipitation can modify fluid flow. Feedback between flow and chemistry can be considered in our model, but the computational burden is increased when such a coupling is included. Alternatively, changes in porosity during the simulation can be monitored by tracking changes in mineral volume fractions without feedback to the fluid flow (as is the case with the present simulations). Permeability changes can then be evaluated by consideration of several alternative models describing the porosity-permeability relationship, including a simple grain model of Kozeny-Carman, as used in the present study, or the model of Verma and Pruess (1988) with a more sensitive coupling of permeability to porosity.

A broad range of subsurface thermal-physical-chemical processes are considered under various thermohydrological and geochemical conditions of pressure, temperature, water saturation, ionic strength, and pH and Eh.  Further details on the process capabilities are given in Xu and Pruess (2001) and Xu et al. (2006).

## 2.2. Geochemical data

The quality and accuracy of geochemical modeling is enhanced through the use of internally consistent and critically evaluated thermodynamic data, derived from a comprehensive review of the published literature. The primary source for equilibrium constants for aqueous species and minerals used in this study originated with the EQ3/6 V7.2b database (Wolery, 1992). However, the thermodynamic properties of several minerals and aqueous species relevant to this study have been revised. To ensure consistency with unmodified equilibrium constants in the EQ3/6 V7.2b database, all revisions were generated by SUPCRT92 (Johnson et al., 1992). A comprehensive revision to the properties of silica polymorphs and $SiO_2(aq)$ was initiated as a result of a recent refinement by Rimstidt (1997). Among the silica polymorphs was opal-A, which is employed in the simulations reported in this paper, and whose thermodynamic properties were determined in part on solubility measurements of biogenic silica reported by Van Cappellen and Qui (1997). The thermodynamic properties of the aqueous species $Fe^{2+}$ and $Fe^{3+}$ and the solubility products of all Fe(II)- and Fe(Ш)- bearing minerals were also corrected according to the work of Parker and Khodakovsky (1995). Solubility products of the feldspars, including oligoclase ($Ca_{0.2}Na_{0.8}Al_{1.2}Si_{2.8}O_8$ or $An_{20}$) are based on the work of Arnorsson and Stefansson (1999). The thermodynamic properties of dolomite and magnesite, siderite and end-member ankerite ($CaFe(CO_3)_2$, and those of the limiting ankerite ideal solid solution composition $CaMg_{0.3}Fe_{0.7}(CO_3)_2$, were revised based on the work of Rock et al. (2001), Preis and Gamsberger (2002), and Chai and Navrotsky (1996). Thermodynamic properties for smectite and illite were modified after Kulik and Aja (1997), and those for chlorite were calculated assuming an ideal binary solid solution based on end-member properties for clinochlore and daphnite by Holland and Powell (1998). Further details are given in Xu et al. (2005).

Reactive chemical-transport modeling requires not only a conceptual understanding of the mechanisms involved in the nucleation, precipitation, and dissolution of the suite of participating minerals, but also quantitative estimates of relevant kinetic parameters. In this paper, a general form of rate expression is used, which is based on transition state theory (TST) (Lasaga et al., 1994; Steefel and Lasaga, 1994):

$$r = kA\left[1 - \left(\frac{Q}{K}\right)^{\theta}\right]^{\eta}$$
(1)

where r is the kinetic rate (positive values indicate dissolution, and negative values precipitation), k is the rate constant (moles per unit mineral surface area and unit time) which is temperature dependent, A is the specific reactive surface area per kg $H_2O$, K is the equilibrium constant for the mineral-water reaction written for the destruction of one mole of mineral, and Q is the reaction quotient. The parameters $\theta$ and $\eta$ must be determined by experiment, but are commonly set equal to unity when experimental quantification is unavailable. The precipitation of secondary minerals is represented using the same kinetic expression as for dissolution.

Recent insights regarding mineral-dissolution kinetics (Lasaga, 1998; Lasaga and Luttge, 2001, 2003) have contributed towards explaining inconsistencies between laboratory experimental determinations of mineral-dissolution kinetics and inferred mineral-alteration rates in the field, e.g., White and Peterson (1990). Other aspects relating to mineral transformation kinetics such as nucleation, the preferential formation and persistence of metastable phases (Steefel and van Capellen, 1990; Ozkan and Ortoleva, 2000) and Ostwald ripening are omitted from the current model. Discussion of their potential impact on the results of the simulations presented in this paper are deferred to Section 5.

For many minerals, the kinetic rate constant k can be summed from three mechanisms (Lasaga et al., 1994; Palandri and Kharaka, 2004):

$$k = k_{nu}^{25} \exp\left[\frac{-E_{nu}}{R}\left(\frac{1}{T} - \frac{1}{298.15}\right)\right] + k_{H}^{25} \exp\left[\frac{-E_{H}}{R}\left(\frac{1}{T} - \frac{1}{298.15}\right)\right] a_{H}^{n_H}$$
$$+ k_{OH}^{25} \exp\left[\frac{-E_{OH}}{R}\left(\frac{1}{T} - \frac{1}{298.15}\right)\right] a_{OH}^{n_{OH}}$$
(2)

where subscripts nu, H, and OH indicate neutral, acid, and base mechanisms, respectively, E is the activation energy, $k^{25}$ is the rate constant at 25°C, R is gas constant, T is absolute temperature, a is the activity of the species; and n is a power term (constant). Notice that parameters $\theta$ and $\eta$ (see Eq. 1) are assumed to be the same for each mechanism, and, for reasons noted above, are set to unity in the present work. The rate constant k can be also dependent on other species. In the present work, the kinetic rate of pyrite dissolution depends on $Fe^{3+}$ and $O_2(aq)$ (see Table 1). Two or more species may be involved in one mechanism. A general form of species dependent rate constants, an extension of Eq. 2, is implemented into TOUGHREACT as

$$ k = k_{nu}^{25} \exp\left[\frac{-E_{nu}}{R}\left(\frac{1}{T} - \frac{1}{298.15}\right)\right] + \sum_i k_i^{25} \exp\left[\frac{-E_i}{R}\left(\frac{1}{T} - \frac{1}{298.15}\right)\right] \prod_j a_{ij}^{n_{ij}} \quad (3) $$

where the subscript i is the index for the additional mechanism, and j is the species index involved in one mechanism.

Mineral dissolution and precipitation rates are a product of the kinetic-rate constant and reactive surface area as represented by Eq. 1. The parameters used for the kinetic rate expression are given in Table 1. Calcite and anhydrite are assumed to react at equilibrium because their reaction rates are rapid relative to the time frame being modeled. In Table 1, we include separate rate constants ($k^{25}$), activation energies (E), and reaction order (n) for processes catalyzed by $H^+$ or $OH^-$. At any pH, the total rate is the sum of the rates from all mechanisms. Catalysis by $H^+$ or $OH^-$ is considered only for mineral dissolution. Parameters for the rate law were taken from Palandri and Kharaka (2004), who compiled and fitted experimental data reported by many investigators.

If the aqueous phase supersaturates with respect to a potential secondary mineral, a small volume faction such as $1 \times 10^{-6}$ is used for calculating the seed surface area for the new phase to grow. The precipitation of secondary minerals is represented using the same kinetic expression as that for dissolution. However, because precipitation rate data for most minerals are unavailable, parameters for neutral pH rates only, as given in Table 1, were employed to describe precipitation. Multiple kinetic precipitation mechanisms can be specified in an input file of the TOUGHREACT program, should such information

become available.

Mineral reactive-surface areas (the second column of Table 1) are based on the work of Sonnenthal et al. (2005), and were calculated assuming a cubic array of truncated spheres constituting the rock framework. The larger surface areas for clay minerals (kaolinite, illite and smectite) are due to smaller grain sizes. In conformity with White and Peterson (1990) and Zerai et al. (2006), a surface roughness factor of 10 is incorporated and defined as the ratio of the true (BET) surface area to the equivalent geometric surface area. Interaction with the minerals is generally expected to occur only at selective sites of the mineral surface, and the actual reactive surface area could be between one and three orders of magnitude less than the surface roughness-based surface area (Lasaga, 1995; Zerai et al. 2006). The difference is attributed to the fact that only part of the mineral surface is involved in the reaction due to coating or armoring, a small area exposed to the brine, and channeling of the reactive fluid flow. To account for these effects, the actual reactive surface areas given in Table 1 are decreased by two orders of magnitude from the surface roughness-based surface areas. The reactive surface areas used here for most minerals are similar to those of Zerai et al. (2006), who used a surface area of 10 $cm^2$/g for all minerals.

The evolution of surface area in natural geologic media is very complex, especially for multi-mineral systems, and is not quantitatively understood at present. The magnitudes of surface areas specified are highly uncertain. We performed sensitivity simulations regarding the rate constants and reactive surface areas to partially address this issue. Details are given in the following two sections.

**Table 1.** Parameters for calculating kinetic rate constants of minerals. Note that: (1) all rate constants are listed for dissolution except opal-A; (2) A is specific surface area, $k^{25}$ is kinetic constant at 25°C, E is activation energy, and n is the power term (Eq. 3); (3) the power terms n for both acid and base mechanisms are with respect to $H^+$, (4) for pyrite, the neutral mechanism has n with respect to $O_2(aq)$, the acid mechanism has two species involved: one n with respect to $H^+$ and another n with respect to $Fe^{3+}$ (see Eq. 3).

| Mineral | $A$ $(cm^2/g)$ | Parameters for kinetic rate law | | | | | | | |
| --- | --- | --- | --- | --- | --- | --- | --- | --- | --- |
| | | Neutral mechanism | | Acid mechanism | | | Base mechanism | | |
| | | $k^{25}$ $(mol/m^2/s)$ | $E$ $(KJ/mol)$ | $k^{25}$ | $E$ | $n(H^+)$ | $k^{25}$ | $E$ | $n(H^+)$ |
| Quartz | 9.1 | $1.023\times10^{-14}$ | 87.7 | | | | | | |
| Kaolinite | 108.7 | $6.918\times10^{-14}$ | 22.2 | $4.898\times10^{-12}$ | 65.9 | 0.777 | $8.913\times10^{-18}$ | 17.9 | -0.472 |
| Illite | 108.7 | $1.660\times10^{-13}$ | 35 | $1.047\times10^{-11}$ | 23.6 | 0.34 | $3.020\times10^{-17}$ | 58.9 | -0.4 |
| Oligoclase | 9.1 | $1.445\times10^{-12}$ | 69.8 | $2.138\times10^{-10}$ | 65 | 0.457 | | | |
| K-feldspar | 9.1 | $3.890\times10^{-13}$ | 38 | $8.710\times10^{-11}$ | 51.7 | 0.5 | $6.310\times10^{-12}$ | 94.1 | -0.823 |
| Na-smectite | 108.7 | $1.660\times10^{-13}$ | 35 | $1.047\times10^{-11}$ | 23.6 | 0.34 | $3.020\times10^{-17}$ | 58.9 | -0.4 |
| Chlorite | 9.1 | $3.02\times10^{-13}$ | 88 | $7.762\times10^{-12}$ | 88 | 0.5 | | | |
| Hematite | 12.9 | $2.512\times10^{-15}$ | 66.2 | $4.074\times10^{-10}$ | 66.2 | 1 | | | |
| Magnesite | 9.1 | $4.571\times10^{-10}$ | 23.5 | $4.169\times10^{-7}$ | 14.4 | 1 | | | |
| Dolomite | 9.1 | $2.951\times10^{-8}$ | 52.2 | $6.457\times10^{-4}$ | 36.1 | 0.5 | | | |
| Low-albite | 9.1 | $2.754\times10^{-13}$ | 69.8 | $6.918\times10^{-11}$ | 65 | 0.457 | $2.512\times10^{-16}$ | 71 | -0.572 |
| Siderite | 9.1 | $1.260\times10^{-9}$ | 62.76 | $6.457\times10^{-4}$ | 36.1 | 0.5 | | | |
| Ankerite | 9.1 | $1.260\times10^{-9}$ | 62.76 | $6.457\times10^{-4}$ | 36.1 | 0.5 | | | |
| Dawsonite | 9.1 | $1.260\times10^{-9}$ | 62.76 | $6.457\times10^{-4}$ | 36.1 | 0.5 | | | |
| Ca-smectite | 108.7 | $1.660\times10^{-13}$ | 35 | $1.047\times10^{-11}$ | 23.6 | 0.34 | $3.020\times10^{-17}$ | 58.9 | -0.4 |
| Alunite | 9.1 | $1.000\times10^{-12}$ | 57.78 | | | | $1.000\times10^{-12}$ | 7.5 | -1.0 |
| Opal-A (dissolution) | 9.1 | $4.900\times10^{-13}$ | 76 | | | | | | |
| Opal-A (precipitation) | 9.1 | $3.800\times10^{-10}$ | 49.8 | | | | | | |
| Pyrite | 12.9 | $k_{25}=2.818\times10^{-5}$ $E_a=56.9$ $n(O_2(aq))=0.5$ | | $k_{25}=3.02\times10^{-8}$ $E_a=56.9$ $n(H^+)=-0.5$, $\quad n(Fe^{3+})=0.5$ | | | | | |

## 3. Problem Setup

### 3.1. Fluid flow conditions

A single-layer uniform sandstone formation with a thickness of 10 m is considered in the present model (Figure 1). Hydrological parameter specifications of the formation are chosen to be representative of those of the Texas Gulf Coast at a depth of about 2 km (Table 2). The formation is assumed to extend infinitely in the horizontal direction. A radial grid is used with spacing that increases away from the well.
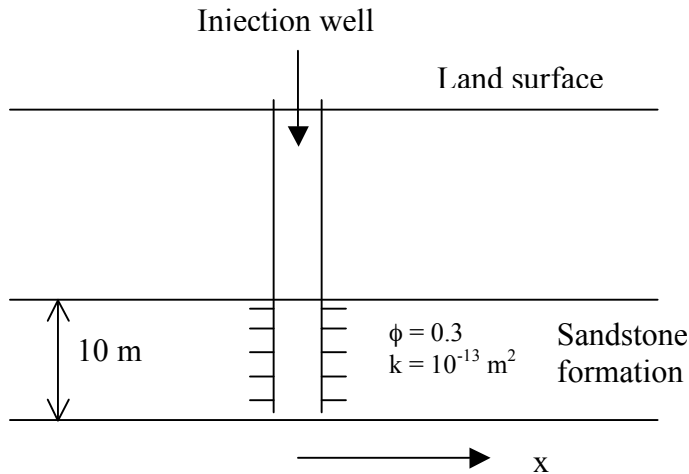


**Figure 1.** Simplified radial flow model for injection of acid gases into a sandstone formation.

This fluid flow simplification does not consider non-uniform sweep that may occur as a result of formation heterogeneities or buoyancy forces that would tend to drive $CO_2$ towards the top of the aquifer. Some justification for a 1-D approach can be derived from the slow rates and long time scales of geochemical changes, which will cause processes to play out over time and make the distribution of $CO_2$ more uniform. Initially, injected $CO_2$ will tend to accumulate and spread out near the top of permeable intervals, partially dissolving in the aqueous phase. $CO_2$ dissolution causes the aqueous-phase density to increase by a few percent, giving rise to buoyant convection where waters

enriched in $CO_2$ will tend to migrate downward (Weir et al., 1995). This $CO_2$ dissolution process and subsequent aqueous-phase convection will tend to mix aqueous $CO_2$ in the vertical direction. The time scale for significant convective mixing is likely to be slow (on the order of hundreds of years or more; Ennis-King and Paterson, 2003), and may be roughly comparable to time scales for significant geochemical interactions of $CO_2$.

The fluid property module ECO2N used in TOUGHREACT considers three components: supercritical $CO_2$, water, and brine. $H_2S$ or $SO_2$ can therefore be co-injected only by separately incorporating these gases in the injected brine. To set up a reasonable simulation, therefore, the $CO_2$ is co-injected with an aqueous-phase equivalent in composition to that of the formation brine with or without additional $H_2S$ or $SO_2$. The average weight ratio of sulfur to carbon in 15 samples of coal used in domestic power plants is approximately 2.5:100 (Apps, 2006, Table 5). Table 3 summarizes the mass flow rates of the injected $CO_2$ and brine with no dissolved gas or with dissolved additions of $H_2S$ or $SO_2$ at concentrations equal to the equivalent carbon to sulfur ratio in the coal. The simulations cannot describe the anticipated condition where an injected anhydrous gas would induce desiccation in the vicinity of the well bore.

**Table 2**. Hydrogeologic parameters for the sandstone formation.

| Parameters | Sandstone |
|---|---|
| Permeability ($m^2$) | $10^{-13}$ |
| Porosity | 0.3 |
| Tortuosity | 0.3 |
| Compressibility ($Pa^{-1}$) | $1 \times 10^{-8}$ |
| Diffusivity ($m^2/s$) | $1 \times 10^{-9}$ |
| Relative permeability | |
| Liquid (van Genuchten, 1980):<br><br>$k_{rl} = \sqrt{S^*} \left\{ 1 - \left( 1 - \left[ S^* \right]^{1/m} \right)^m \right\}^2$<br><br>$S_{lr}$ : irreducible water saturation<br>m: exponent | $S^* = (S_l - S_{lr})/(1 - S_{lr})$<br><br><br>$S_{lr} = 0.3$<br>$m = 0.457$ |
| Gas (Corey, 1954):<br><br>$k_{rg} = (1 - \widehat{S})^2 (1 - \widehat{S}^2)$<br><br><br>$S_{gr}$ : irreducible gas saturation | $\widehat{S} = \dfrac{(S_l - S_{lr})}{(S_l - S_{lr} - S_{gr})}$<br><br><br>$S_{gr} = 0.05$ |
| Capillary pressure | |
| van Genuchten (1980)<br>$P_{cap} = -P_0 \left( \left[ S^* \right]^{-1/m} - 1 \right)^{-m}$<br><br>$S_{lr}$ : irreducible water saturation<br>m: exponent<br>$P_0$ : strength coefficient | $S^* = (S_l - S_{lr})/(1 - S_{lr})$<br><br><br>$S_{lr} = 0.00$<br>$m = 0.457$<br>$P_0 = 19.61\,kPa$ |

**Table 3.** Fluid mass injection rates (kg/s) over 10 m thick sandstone aquifer layer.

| Case | $CO_2$ | Water | $H_2S$ | $SO_2$ |
|---|---|---|---|---|
| $CO_2$ only | 1 | 0.5 | | |
| $CO_2$ with $H_2S$ | 1 | 0.4807 | 0.0193 | |
| $CO_2$ with $SO_2$ | 1 | 0.4636 | | 0.0364 |

## 3.2. Initial geochemical conditions

The initial mineral composition of the quartzose lithic arkose used in the present modeling (Table 4) is similar to Xu et al. (2004). Details on the selection of mineral composition are given in Xu et al. (2005). Because $H_2S$ and $SO_2$ are respectively injected in addition to $CO_2$, potential secondary sulfates such as anhydrite and alunite were included. Gypsum is excluded, because it is unstable with respect to anhydrite at the formation temperature of $75^{\circ}C$. In addition, only opal-A among the silica polymorphs is allowed to precipitate. The persistence of metastable silica polymorphs in nature is well known. A rough estimate of the time required to transform opal-A to opal-CT at 75°C can be made based on interpolation of estimated times to transform a substantial fraction of opal-A to opal-CT in argillaceous oceanic sediments as a function of temperature (Kastner, 1979). These data and experimental data at 150° by Kastner et al. (1977) on the formation of opal-CT in seawater and at 300°C by Siffert and Wey (1967) for the transformation time of amorphous silica to cristobalite, suggest that this transformation would take approximately 4,500 years at 75°C. The transformation of opal-CT to quartz in sediments undergoing diagenesis at 60-150°C appears to take place over even longer times, perhaps on the order of a million years, and may be coupled to the long-term persistence of co-existing smectites (Abercrombie et al., 1994). Therefore it is reasonable to assume that opal-A or a similar poorly crystalline silica polymorph would most likely persist and control $SiO_2$(aq) activity over the initial 5,000 years of the simulation, but that opal-CT would predominate by 10,000 years.

**Table 4.** Initial mineral volume fractions and possible secondary mineral phases used in the simulations.

| Mineral | Chemical formula | Volume percent | |
|---|---|---|---|
| | | *of solid* | *of medium* |
| | | | |
| ***Primary***: | | | |
| Quartz | $SiO_2$ | 58 | 40.6 |
| Kaolinite | $Al_2Si_2O_5(OH)_4$ | 2.02 | 1.41 |
| Calcite | $CaCO_3$ | 1.93 | 1.35 |
| Illite | $K_{0.6}Mg_{0.25}Al_{1.8}(Al_{0.5}Si_{3.5}O_{10})(OH)_2$ | 1.0 | 0.7 |
| Oligoclase | $Ca_{0.2}Na_{0.8}Al_{1.2}Si_{2.8}O_8$ | 19.8 | 13.86 |
| K-feldspar | $KAlSi_3O_8$ | 8.2 | 5.74 |
| Na-smectite | $Na_{0.290}Mg_{0.26}Al_{1.77}Si_{3.97}O_{10}(OH)_2$ | 4 | 2.8 |
| Chlorite | $Mg_{2.5}Fe_{2.5}Al_2Si_3O_{10}(OH)_8$ | 4.55 | 3.19 |
| Hematite | $Fe_2O_3$ | 0.5 | 0.35 |
| Porosity | | ---- | 30 |
| ***Secondary***: | | | |
| Anhydrite | $CaSO_4$ | | |
| Magnesite | $MgCO_3$ | | |
| Dolomite | $CaMg(CO_3)_2$ | | |
| Low-albite | $NaAlSi_3O_8$ | | |
| Siderite | $FeCO_3$ | | |
| Ankerite | $CaMg_{0.3}Fe_{0.7}(CO_3)_2$ | | |
| Dawsonite | $NaAlCO_3(OH)_2$ | | |
| Ca-smectite | $Na_{0.145}Mg_{0.26}Al_{1.77}Si_{3.97}O_{10}(OH)_2$ | | |
| Alunite | $KAl_3(OH)_6(SO_4)_2$ | | |
| Pyrite | $FeS_2$ | | |
| Opal-A | $SiO_2$ | | |

Prior to simulating reactive transport, batch geochemical modeling of water-rock interaction was performed to generate an aqueous-phase chemical composition closely approaching the composition of a typical formation brine by equilibrating a 1.0 molal ($m$, mol/kg $H_2O$) solution of sodium chloride in the presence of the primary minerals listed in Table 4 (with $CO_2$ gas pressure of 0.1 bar at a temperature of $75°C$). A reasonably short simulation time (10 years in the present study) is needed to obtain a quasi-stable (or nearly steady-state) aqueous solution composition (Table 5).

**Table 5.** Initial total dissolved component concentrations for reactive transport simulations. Iron is the sum of $Fe^{2+}$, $Fe^{3+}$ and their related complexes. Carbon is the sum of $CO_2(aq)$, $CH_4(aq)$, and their related species such as $HCO_3^-$ and acetic acid(aq). Sulfur is the sum of sulfate and sulfide species. Ionic strength is 1.06. Activity coefficients of aqueous species are calculated from the extended Debye-Hückel equation (Helgeson et al., 1981).

| Component | Concentration | |
|---|---|---|
| | *(mol/kg H₂O)* | *(ppm)* |
| $Ca^{2+}$ | $6.23 \times 10^{-2}$ | 250 |
| $Mg^{2+}$ | $3.69 \times 10^{-6}$ | 0.09 |
| $Na^+$ | 0.99 | 22800 |
| $K^+$ | $6.07 \times 10^{-3}$ | 237 |
| Iron | $1.58 \times 10^{-4}$ | 0.16 |
| $SiO_2(aq)$ | $9.02 \times 10^{-4}$ | 54.2 |
| Carbon | $5.04 \times 10^{-2}$ | 6.05 |
| Sulfur | $1.32 \times 10^{-9}$ | 0.00004 |
| $Al^{3+}$ | $1.56 \times 10^{-8}$ | 0.0004 |
| $Cl^-$ | 1.0 | 35500 |
| $O_2(aq)$ | $8.81 \times 10^{-66}$ | - |
| | | |
| pH | 6.7 | |
| Temperature | 75°C | |

## 3.3 Simulations

Two groups of simulations were performed. The first of three simulations corresponds to the combinations of injected gases given in Table 3 (acid-gas simulations). The second group of three simulations examined sensitivities to reaction rates by decreasing the magnitude of the rate constant (or surface area) of oligoclase, chlorite, and Opal-A each by one order of magnitude.

In all simulations, the initial reservoir pressure was set at a constant 200 bar with a formation temperature of 75°C. This temperature is calculated for a depth of 2 km, given a land surface temperature of 15°C and a geothermal gradient of 30°C/km.

Continuous injection was assumed to take place over a period of 100 years. Thereafter, geochemical transport simulations were continued until 10,000 years. Because the arkose layer is uniform, the present simulations do not model non-uniform sweep effects that may occur in heterogeneous formations. Furthermore, buoyancy forces that would tend to drive gases towards the top of the sandstone are also not taken into account in the model. The consequences of these limitations are discussed in Section 5.

## 4. Results

## 4.1 Acid-gas simulations

The output of the simulations conducted for this study is very extensive, essentially consisting of three categories of information: (1) the aqueous phase composition, (2) the distribution of primary and secondary minerals, and (3) the physical properties of the system (such as porosity). For convenience, we present selected information in graphical form as a function of radial distance from the well bore, and at discrete time intervals of 10, 100, 1,000, and 10,000 years. Although the objective of this study is to assess the impact of either $H_2S$ or $SO_2$ on the distribution and extent of $CO_2$ sequestration through precipitation of secondary carbonates, it must be emphasized that the magnitude and extent of destruction of primary minerals, and the formation of secondary clays, is of considerable importance when model comparisons are made with analogous natural systems. For this reason, in Appendix A we include supplementary information regarding the alteration of primary minerals and formation of secondary minerals. The fluid flow pattern (water and gas saturations) obtained from all three simulations is similar and is also presented in Appendix A (Figure A-1).

The pH distributions along the radial distance are presented in Figure 2. For the $CO_2$ only case (Figure 2a), pH reaches 3.9 close to the injection well after 10 years. The injected $CO_2$ causes the pH to trend lower, but calcite dissolution consumes $H^+$ and increases pH. After 100 years when the injection ceases, the effects of mineral alteration cause pH to increase, and after 1,000 years, a pH of about 6 is attained. For the case of

CO$_2$ with H$_2$S (Figure 2b), a minimum pH of 3.65 is obtained close to the well, which is slightly lower than the CO$_2$-only case. After 100 years, the pH distribution corresponds closely with that of the case with CO$_2$ alone.



(a) CO$_2$ Only          (b) CO$_2$ + H$_2$S          (c) CO$_2$ + SO$_2$
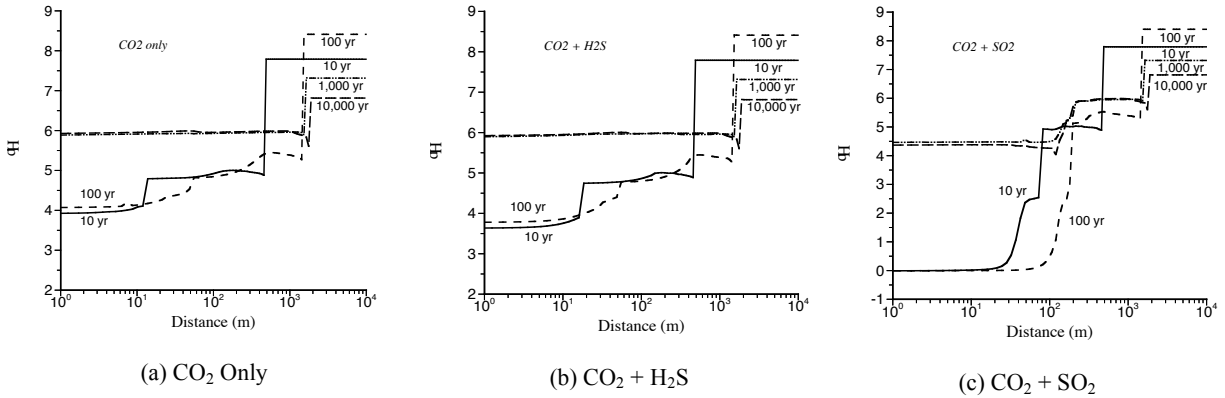
**Figure 2**. The pH at different times after initiating injection.

Extremely acidic conditions (with a pH close to zero) result from injection of SO$_2$ (Figure 2c), because the model assumes that SO$_2$ instantly disproportionates with generation of sulfuric acid and hydrogen sulfide (Kusakabe et al., 2000; Knauss et al., 2005):

$$4SO_2 + 4H_2O \rightarrow 3H_2SO_4 + H_2S \qquad (4)$$

The low pH is maintained until injection ceases after 100 years, by which time the extremely acidified zone extends to a radial distance of over 100 m. As expected, concentrations of sulfate and sulfide increase (Figure 3). Calcite rapidly disappears within this zone, leading to anhydrite precipitation (Figure 4a). The generation of sulfuric acid also leads to precipitation of alunite (Figure 4b). Precipitation of these two minerals immobilizes most sulfate generated during the initial injection period. Although some anhydrite precipitates within 200 m, most sulfate is immobilized through alunite precipitation in the region between 50 - 150 m, with a peak volume fraction of 7% at about 100 m distance.

20
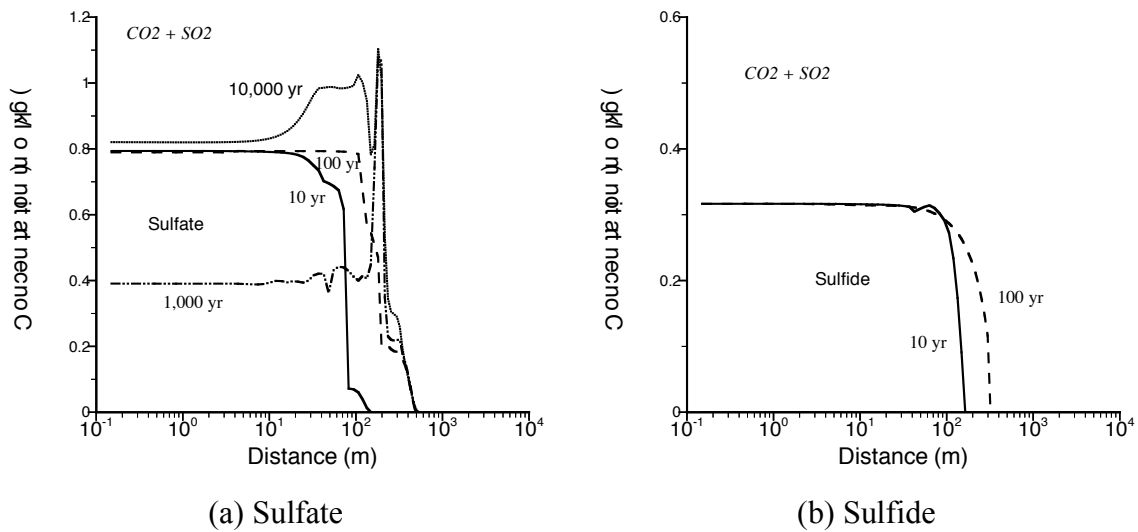
(a) Sulfate                           (b) Sulfide

**Figure 3**. Aqueous concentrations of sulfate and sulfide at different times for the $CO_2+SO_2$ injection case.



(a) Anhydrite                        (b) Alunite
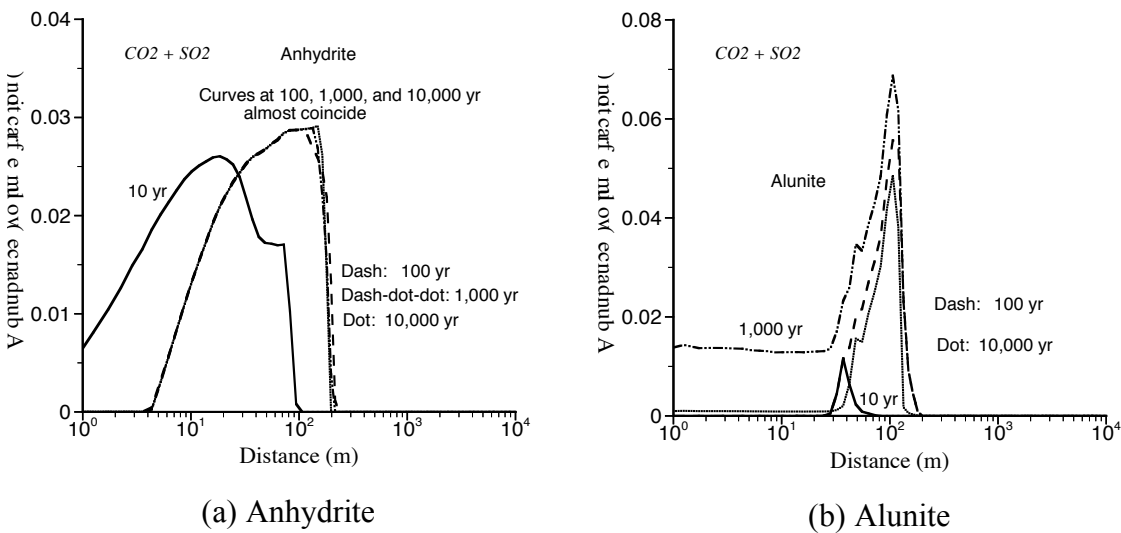
**Figure 4**. Abundances (volume fraction) of anhydrite and alunite at different times for the $CO_2+SO_2$ injection case. Note that for anhydrite curves at 100, 1,00, and 10,000 yr almost coincides, indicating that anhydrite stabilizes after 100 yr.

The injection of both $H_2S$ and $SO_2$ causes pyrite precipitation (Figure 5). For the $H_2S$ case, the abundances of pyrite after 1,000 years remain constant (the curve at 10,000 yr coincides with that at 1,000 yr). For $SO_2$ co-injection, the pyrite abundances at 10,000 years are slightly lower than those at 1,000 years. For the $H_2S$ co-injection, the dissolved $H_2S$ (sulfide) was elevated during the injection period of 100 years (Figure 6), but is later attenuated through pyrite precipitation. Essentially no sulfide is present in the aqueous phase after 1,000 years. Therefore, no curves for 1,000 and 10,000 years are presented in Figure 6. During $SO_2$ co-injection, the aqueous sulfide concentration in solution is insignificant.



(a) $CO_2 + H_2S$            (b) $CO_2 + SO_2$
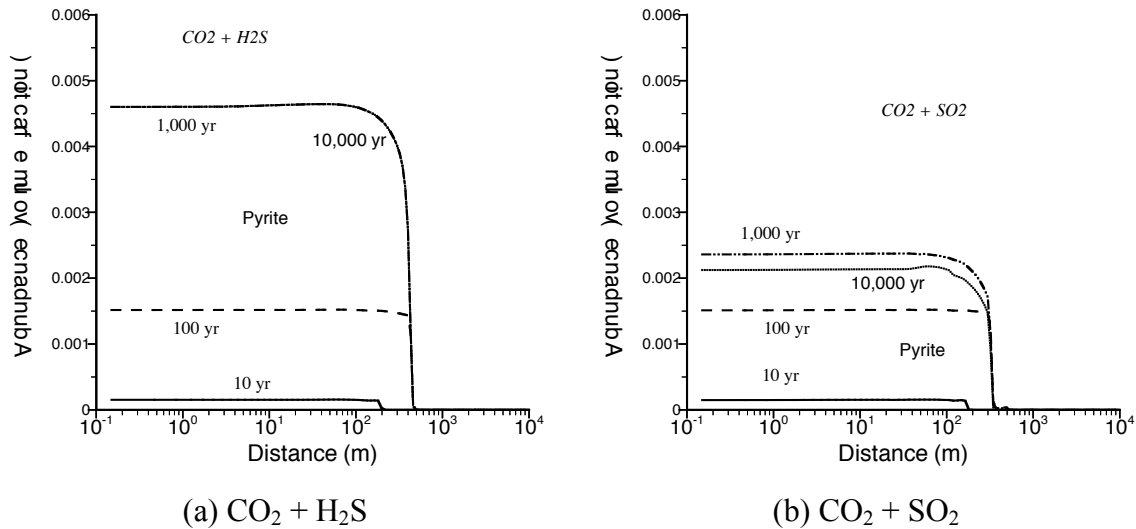
**Figure 5**. Abundances of pyrite at different times with injection of (a) $H_2S$, and (b) $SO_2$.
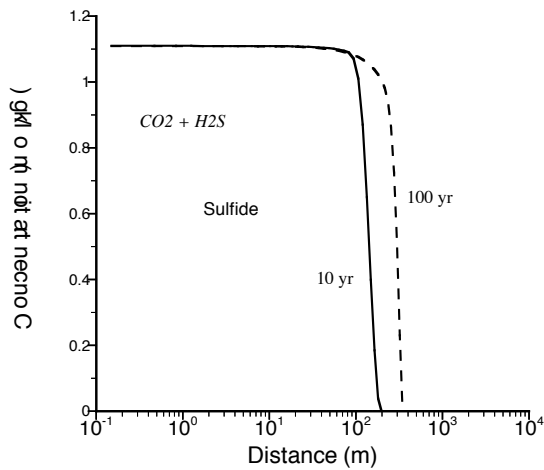
**Figure 6**. Aqueous concentration of sulfide at different times for the $CO_2+H_2S$ injection case.

We now address mineral alteration and carbonate precipitation induced by the injected $CO_2$. The results obtained from the injection of $CO_2$ alone are very similar to those involving the injection of $CO_2$ with $H_2S$. Therefore only the results from the injection of $CO_2$ alone will be compared with those for $CO_2$ with co-injected $SO_2$.

Alteration surrounding the well bore differs both in the nature and in the extent of secondary mineral formation, depending on whether the acidity caused by the introduction of injected gases is moderate (as with the injection of $CO_2$ alone or $CO_2$ with minor $H_2S$, or severe when minor $SO_2$ is co-injected with $CO_2$. This is illustrated respectively with distributions of secondary Opal-A and Na-smectite in Figures 7 and 8. Precipitation of opal-A is extensive in both cases (Figure 7). Maximum opal-A precipitation occurs with the co-injection of $SO_2$, having a peak value of 17% volume at a distance of 30 m. With $CO_2$ alone, precipitation of Na-smectite is extensive within the entire plume of injected $CO_2$ (Figure 8), but with $CO_2 + SO_2$ injection, the precipitation of Na-smectite is insignificant in the acidified zone within 100 m of the well bore.
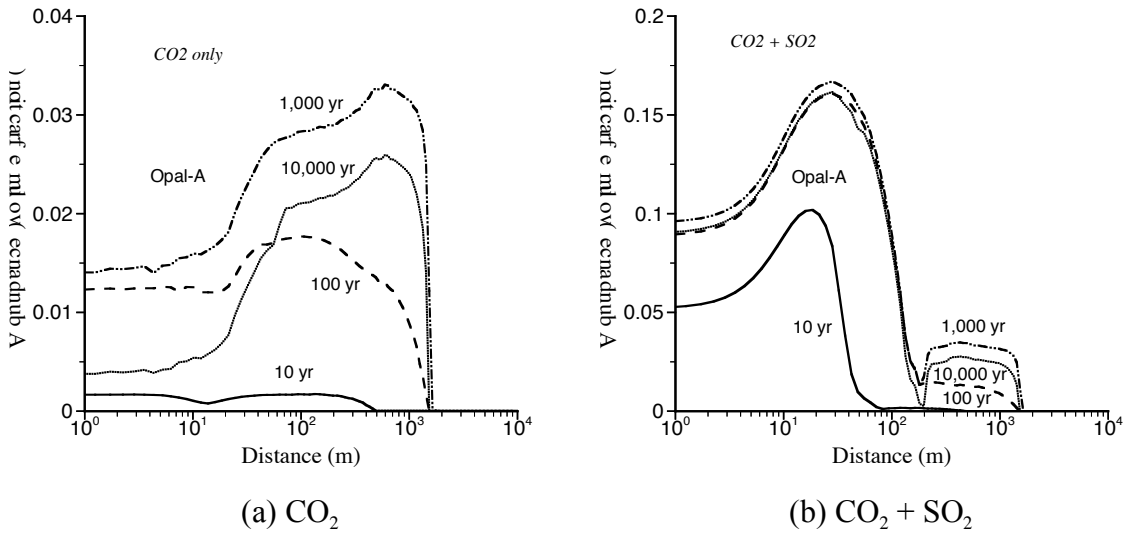
**Figure 7**. Variation of opal-A abundance with time.
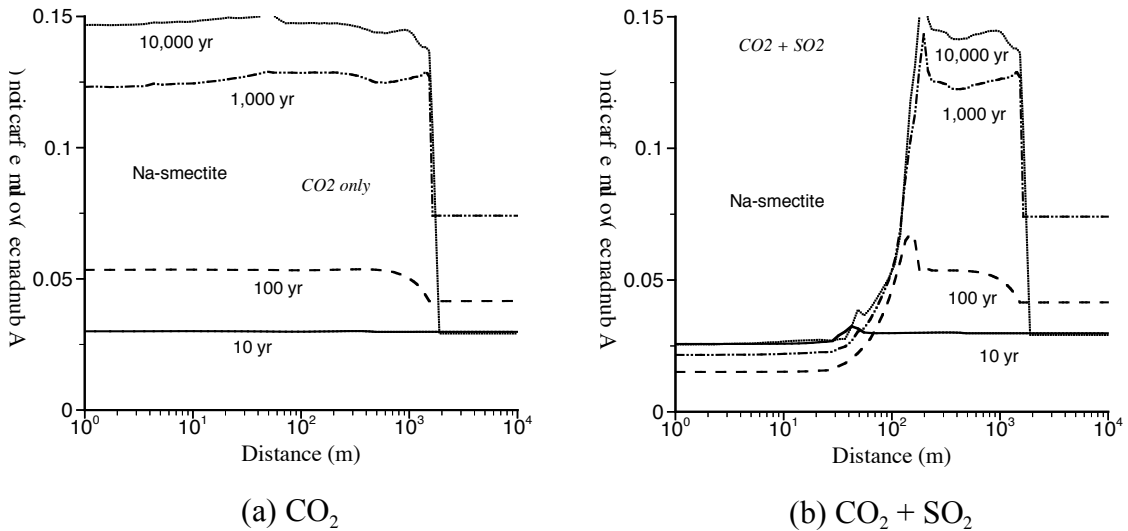


**Figure 8**. Variation of Na-smectite abundance with time.

The simulated formation of secondary carbonates calcite, ankerite and dawsonite is illustrated in Figures 9-11. Although calcite was initially present in the formation, it is completely destroyed up to a radius of over 50 m from the well bore when $CO_2$ alone is injected (Figure 9). With co-injection of $SO_2$, calcite destruction extends even further, to approximately 100 m. Although a small amount of calcite precipitation occurs

downstream of the primary dissolution front, its contribution to $CO_2$ sequestration is small when compared to other carbonates. In the region unaffected by the injection, calcite continues to precipitate as a consequence of oligoclase corrosion. The preponderant minerals sequestering $CO_2$ are ankerite (Figure 10) and dawsonite (Figure 11). Ankerite appears after 100 years, and about a 3.5% volume fraction of ankerite is formed after 10,000 years in a zone ranging from 100 to 1,600 m. When $SO_2$ is co-injected, ankerite precipitation is inhibited within the acidified zone. However, it does precipitate in significant amounts together with dawsonite in the region immediately peripheral to the acidified zone, each occupying volume fractions of about 3%. No dolomite precipitation is observed. Trace amount of magnesite precipitates in the acidified zones close to the well bore. Small amount of siderite also precipitates in the zone beyond a 100 m distance.



(a) $CO_2$                                        (b) $CO_2 + SO_2$
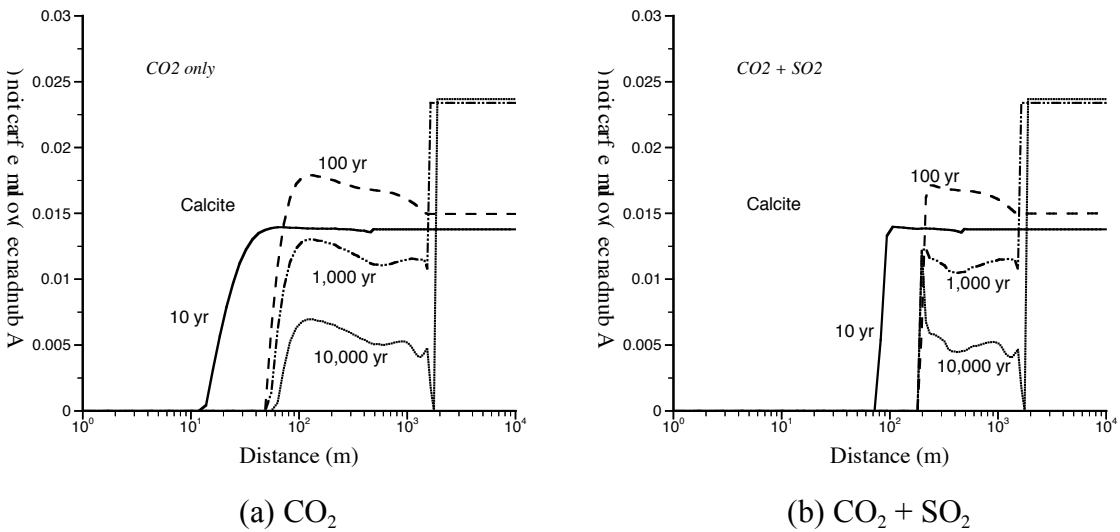
Figure 9. Variation of calcite abundance with time.
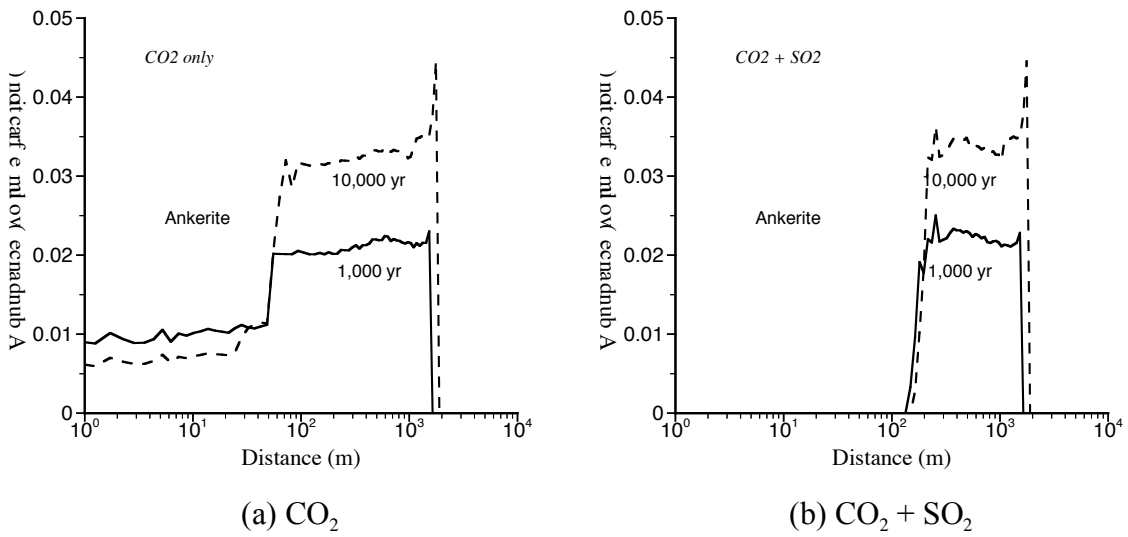
Figure 10. Variation of ankerite abundance with time.
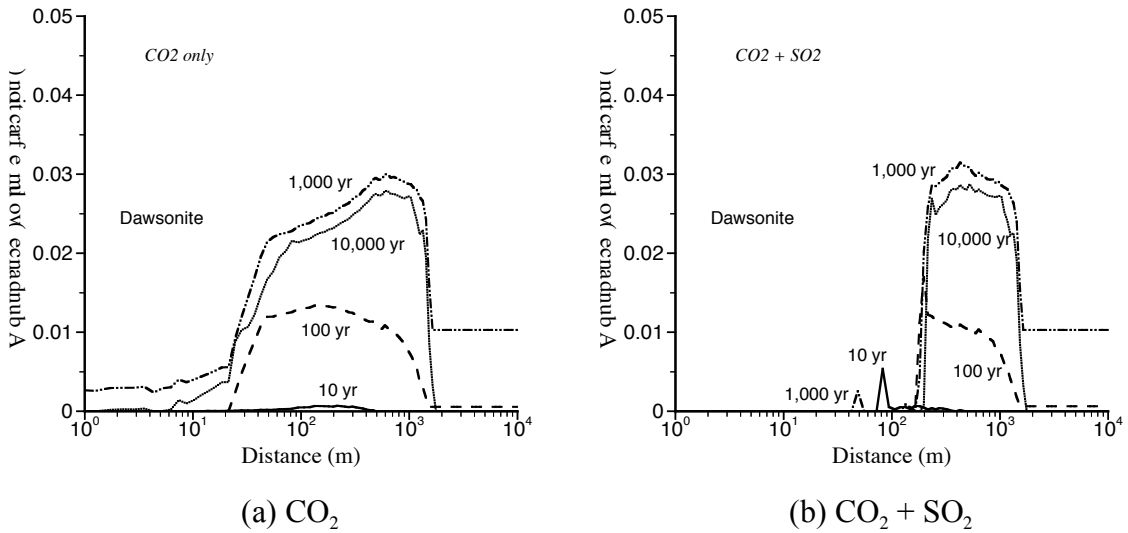


**Figure 11**. Variation of dawsonite abundance with time.

The total quantity of $CO_2$ sequestered in minerals, mainly as ankerite and dawsonite, with small amounts of siderite, is presented in Figure 12. As expected, no $CO_2$ is sequestered in mineral phases in the acidified zone during injection, instead some negative amount of $CO_2$ is sequestered (not shown in Figure 12) because calcite

dissolves. After injection ceases at 100 years, only small quantities of $CO_2$ are sequestered through carbonate precipitation within the acidified zone surrounding the well bore. $CO_2$ mineral sequestration occurs primarily beyond the acidified zone (after pH rises). Fe(II) for siderite and ankerite precipitation is supplied by chlorite and by reduction of Fe(III) in small amounts of hematite (Figure A-4 in Appendix A). Precipitation of dawsonite requires $Na^+$ provided by oligoclase dissolution, which also supplies Ca for ankerite and Al for dawsonite. Essentially no $Na^+$ is provided from sodium chloride in the brine (see Figure 14). The initial abundance of chlorite and oligoclase therefore affects $CO_2$ mineral-trapping capability. The sequestration time required depends on the kinetics of mineral dissolution and precipitation.
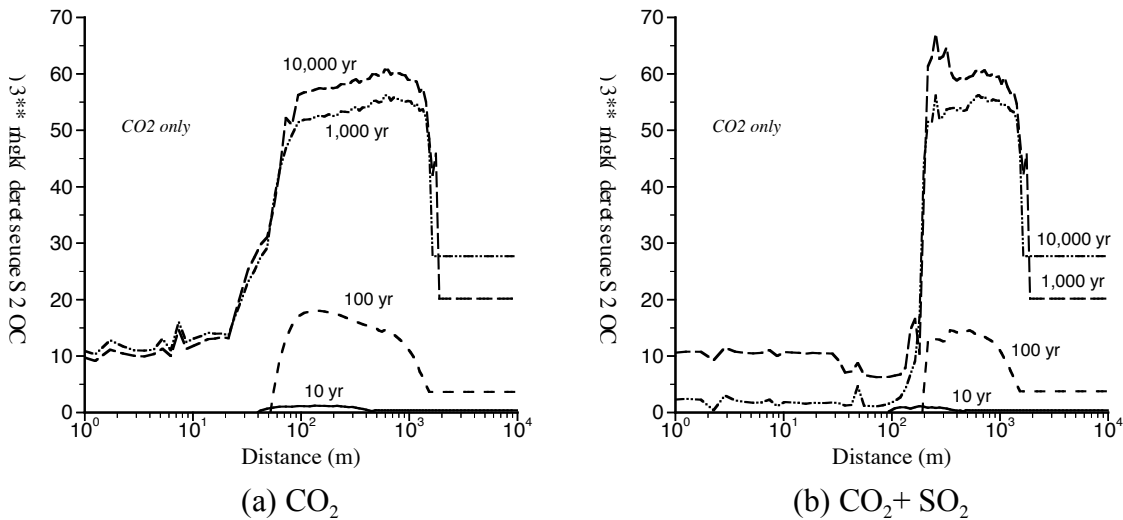


**Figure 12**. Cumulative sequestration of $CO_2$ by carbonate minerals with time.

The zonal distribution of carbonates and sulfates reflects the pH distribution. Carbonates are stable at higher pH (around 6), whereas the sulfate minerals anhydrite and alunite are stable at lower pH (i.e., 4-5) within about 200 m of the well bore.

Significant changes in porosity occur (Figure 13), especially in the acidified zones where mineral dissolution dominates. With co-injection of $SO_2$, the porosity in the

acidified zone increases from an initial 0.3 to 0.43 after 100 years, which could result in mechanical compaction. However, within the region where carbonate precipitation is at a maximum, the porosity decreases to about 0.275 for both cases. The precipitation of sulfates decreases the porosity to a local minimum of 0.225 about 100 m from the well bore, coinciding with the maximum precipitation of alunite (Figure 4b).
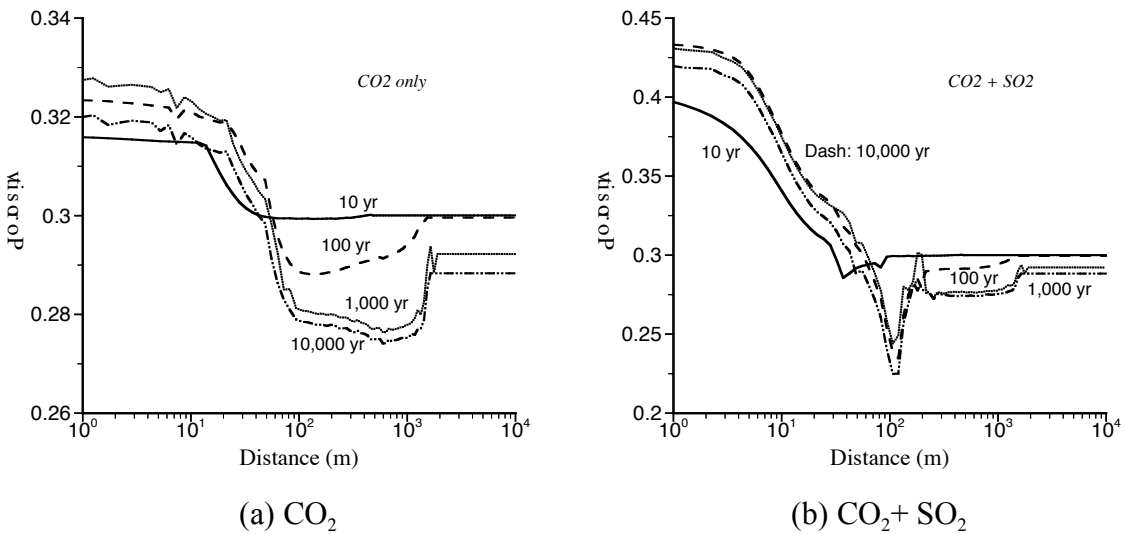


**Figure 13**. Porosity distribution at different times.

As oligoclase dissolves (Figure A-2 in Appendix A), the total dissolved concentration of $Na^+$ increases gradually (Figure 14). With $CO_2$ alone, a maximum $Na^+$ concentration of 2.6 mol/kg is obtained, but with added $SO_2$, the $Na^+$ concentration increases to 3 mol/kg. Concentrations of total dissolved carbonate (mainly $HCO_3^-$) also increase through aqueous complexation, mainly with $Na^+$, increasing $CO_2$ uptake in the aqueous phase. In the acidified zone of the $CO_2 + SO_2$ case, the total dissolved $Na^+$ concentration is only 1 Molar. This is because the $Na^+$ bearing mineral oligoclase is completely dissolved in this region and flushed outward by injected brine.
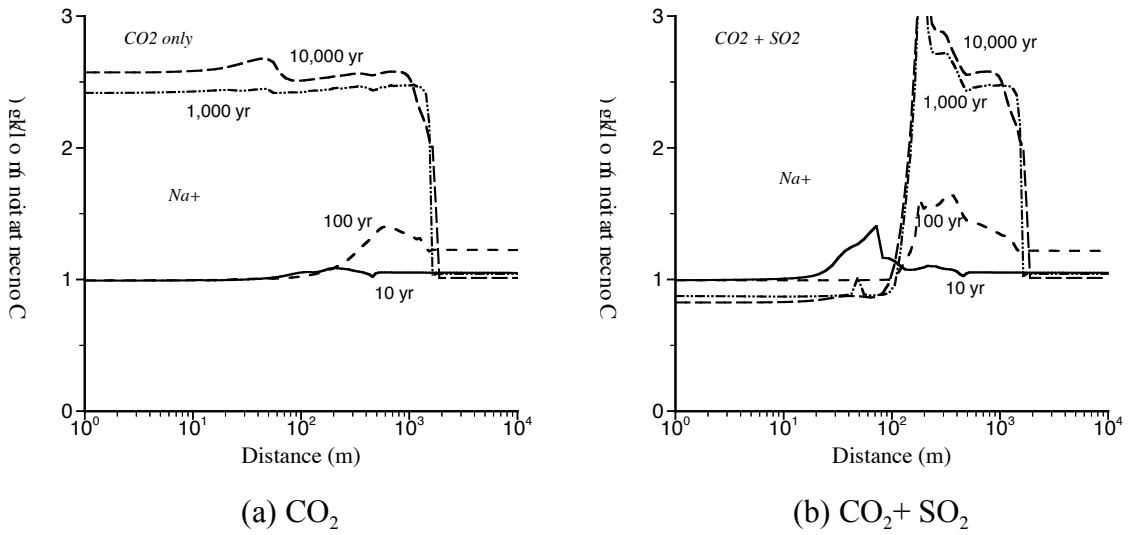
**Figure 14**. Aqueous concentration of $Na^+$ at different times.
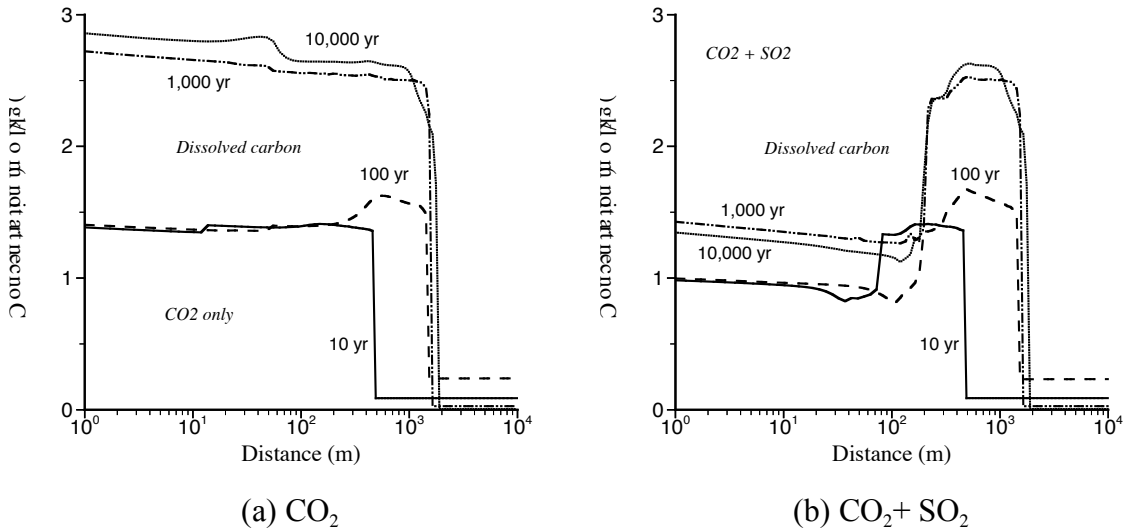


**Figure 15**. Aqueous concentrations of dissolved carbon (mainly $HCO_3^-$) at three different times.

## 4.2. Sensitivity Tests

The purpose of the sensitivity tests is to assess how uncertainties in mineral dissolution rates affect the alteration pattern of the system and $CO_2$ mineral sequestration.

The time required for sequestration depends on the rates of mineral dissolution and precipitation, which are products of the kinetic rate constant and reactive surface area. As noted by Xu et al. (2004), scaling the dissolution and precipitation rates for all minerals by the same factor is equivalent to reciprocal scaling of the time coordinate. Xu et al. (2005) examined the sensitivity of dawsonite precipitation to changes in the dissolution and precipitation rate constants. Decreases in the rate constant by two and three orders of magnitude resulted in only small changes in the precipitation rate, because dawsonite precipitation is substantially controlled by the slow dissolution of aluminosilicate mineral precursors.

Previous studies also showed that initial abundances of chlorite and oligoclase dominated the $CO_2$ mineral-trapping capability of the aquifer host rock (Xu et al., 2005). Therefore, the $CO_2$ sequestration rate is primarily a function of dissolution kinetics of chlorite and oligoclase. To examine the sensitivity of $CO_2$ sequestration to chlorite and oligoclase dissolution kinetics, we performed three additional simulations by individually decreasing the rate constants for chlorite, oligoclase, and opal-A by two orders of magnitude. The sensitivity simulations were conducted with $CO_2$ injection alone, referred to subsequently as the base-case.

We present simulated changes in mineral abundance over time at 500 m distance from the borehole within the $CO_2$ mineral-trapping zone. Results obtained from the three sensitivity simulations are compared to the base-case with $CO_2$ injection alone and summarized in Table 6. The lower chlorite dissolution rate limits $Mg^{2+}$ and $Fe^{2+}$ supply. Consequently, the quantity of secondary Na-smectite precipitation decreases (compare Figure 16b to 16a), a trace of siderite precipitates (Figure 17b), and ankerite no longer forms. Dawsonite and calcite precipitation increase slightly (compare Figure 17b to 17a). The total quantity of $CO_2$ sequestered by carbonate minerals is slightly lower than in the base-case (Figure 18). The simulated changes of some aqueous concentrations are presented in Figures B-1 and B-2 in Appendix B. With the exception of the case in which opal-A rates were lowered, $Na^+$ and $HCO_3^-$ concentrations generally increase over time, enhancing $CO_2$ sequestration in the saline pore water.

**Table 6.** List of results of sensitivity simulations compared to the base-case (with $CO_2$ injection alone).

| Sensitivity simulation | Mineral alteration | $CO_2$ mineral trapping |
|---|---|---|
| Lower chlorite dissolution rate | Decrease $Mg^{2+}$ and $Fe^{2+}$ supply. Decrease Na-smectite and siderite precipitation. No ankerite formed. Increase slightly dawsonite and calcite precipitation | Slightly lower |
| Oligoclase dissolution rate | Evolution of secondary carbonate minerals is more complex. Precipitation of dawsonite commences after 4,000 years. Calcite initially dissolves, but then re-precipitates after 4,000 years. Ankerite initially forms, but then redissolves after 700 years, then forms again, attaining a maximum concentration after 4000 years, but then declines in concentration as dawsonite, and calcite make an appearance. | Much lower |
| Opal-A precipitation rate | Lesser dawsonite precipitation and greater ankerite precipitation | Lower |
| New rate Law | Steady dissolution of oligoclase and precipitation of Na-smectite and carbonate minerals. Much less dawsonite precipitates due to slower dissolution of aluminosilicate minerals especially oligoclase. | Lower and steady |

When the oligoclase dissolution rate is decreased by two orders of magnitude, Na-smectite remains as a secondary precipitate (compare Figure 16c to 16a). However, evolution of secondary carbonate minerals is more complex (Figure 17c). Precipitation of dawsonite commences after 4,000 years (compare Figure 17c to 17a). Calcite initially dissolves, but then re-precipitates after 4,000 years. Ankerite initially forms, but then redissolves after 700 years. It then forms again, attaining a maximum concentration after 4,000 years, but then declines in concentration as dawsonite and calcite make an appearance. Decreasing the precipitation rate of opal-A by two orders of magnitude results in lesser dawsonite precipitation and greater ankerite precipitation (Figure 17d). Overall, the quantity of $CO_2$ sequestered by secondary carbonates is lower than in the base-case (Figure 18).
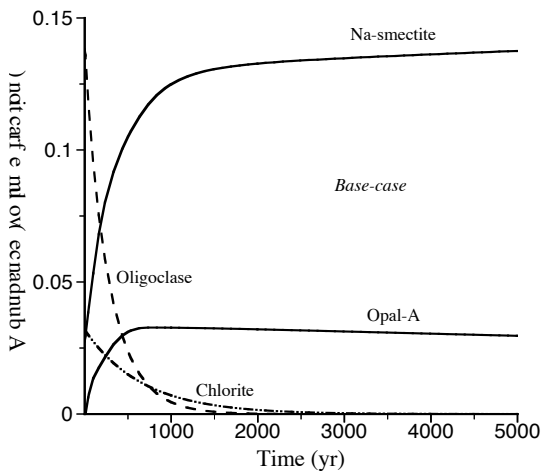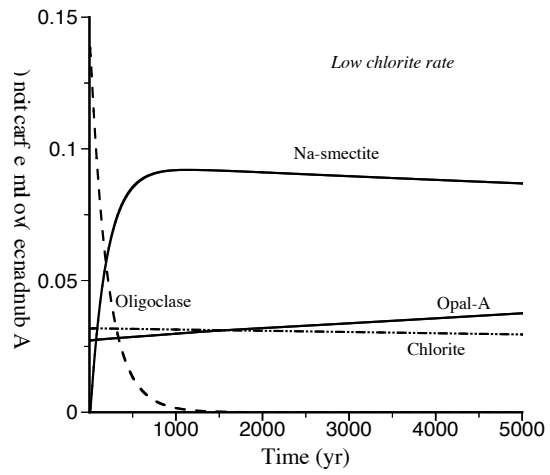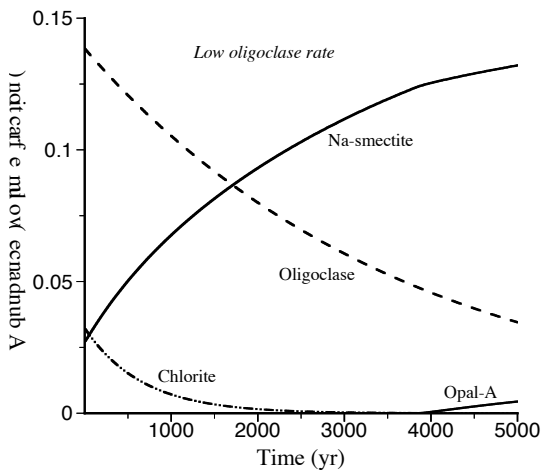
**Figure 16**. Evolution of chlorite, oligoclase, Na-smectite, opal-A, and Na-smectite abundances at 500 m distant from the borehole for sensitivity simulations.
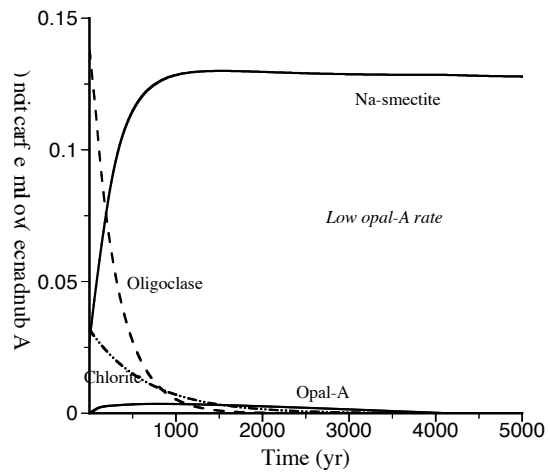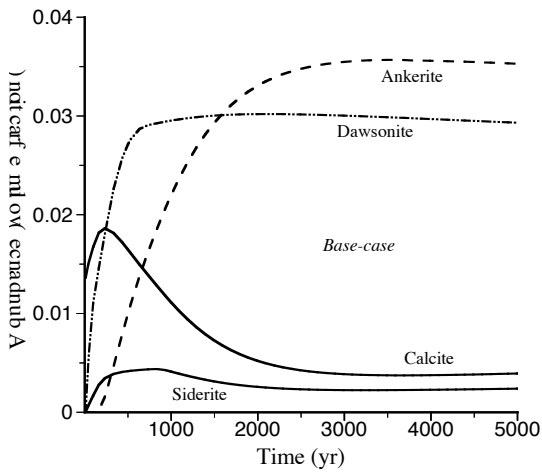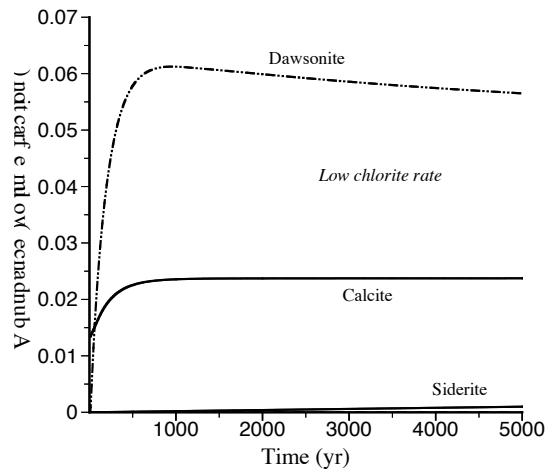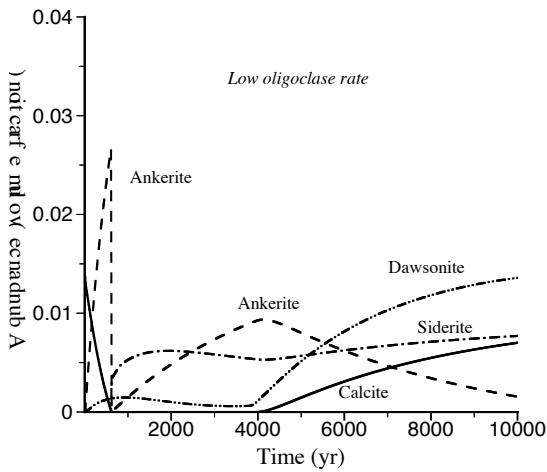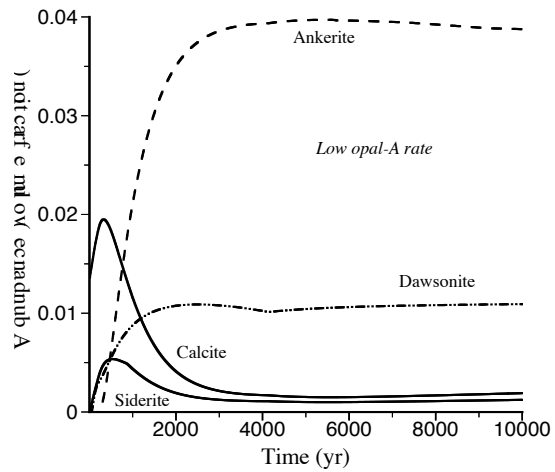
(a) Base-case

(b) Low chlorite dissolution rate

(c) Low oligoclase dissolution rate

(d) Low opal-A precipitation rate

**Figure 17**. Evolution of ankerite, dawsonite, siderite, and calcite abundances at 500 m distant from the borehole for sensitivity simulations.
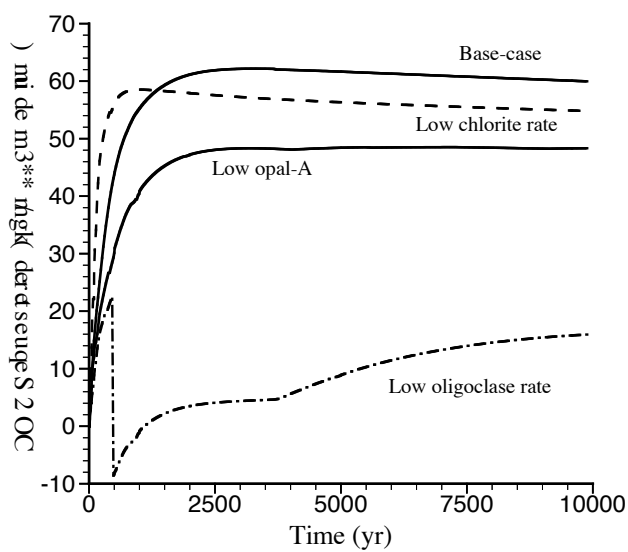
**Figure 18**. $CO_2$ sequestered with time by secondary carbonate mineral for sensitivity simulations (500 m distant from the borehole).

## 5. Model Limitations

The simulations presented in this paper provide valuable insights regarding the chemical consequences of co-injecting gaseous $H_2S$ and $SO_2$ with $CO_2$ in the subsurface environment. The results are, however, constrained by the limitations of current reactive chemical transport simulators to replicate all of the complex physical, hydrological and geochemical processes that are expected to occur, but have not been incorporated in the underlying models.  Some omissions can be justified, because they would not contribute significantly to elucidating the processes under investigation; others, while important, would require a more detailed comprehension of hydrological or chemical processes and quantification of relevant physical, kinetic, and thermodynamic parameters than are currently available.  In other words, more experimental studies and further model and code development are needed to fill the gaps in our knowledge. In the following paragraphs, we discuss some of the principal simplifications and how their rectification might affect the findings presented in this paper.  The simplifications can be divided into two broad categories: hydrological and geochemical.

The current model is limited in that only $CO_2$ can be injected in the gaseous state. Therefore, the co-injection of a brine carrying dissolved gaseous $H_2S$ or $SO_2$ was required

34

as an artifact of the simulation. The consequences of this artifact on the model results, especially in relation to $CO_2$ sequestration, are relatively minor because injection occurs only in the first 100 years, much shorter than the simulation time of 10,000 years. However, the current model cannot replicate desiccation around the well bore during injection. The geochemical consequences, especially in relation to the interaction of $SO_2$ and the products of disproportionation in the injection zone immediately surrounding the well bore, must await future study. Fluid flow modeling capabilities for injection of anhydrous supercritical $CO_2$ containing either $H_2S$ or $SO_2$ gases are under development.

Precipitating secondary carbonates consume aqueous $CO_2$, with a consequential decrease in gas phase saturation and pressure. In the flow equations, these sink terms were not taken into account, because of the computational demand of the long simulation. To examine the coupling effect of reaction sink terms, we performed two batch simulations, uncoupled and coupled, using conditions similar to the $CO_2$ trapping zone at a 500 m radius ($CO_2$-only case with a lower chlorite dissolution rate). The resulting $CO_2$ sequestrations over time are presented in Figure 19. As expected, the coupled case has a slightly lower quantity of $CO_2$ sequestered in mineral phases. After 1,500 years, about 45 kg/m$^3$ medium is sequestered, but sequestration progresses slowly thereafter, because of the progressive depletion of a separate $CO_2$ gas phase and primary reactive minerals).
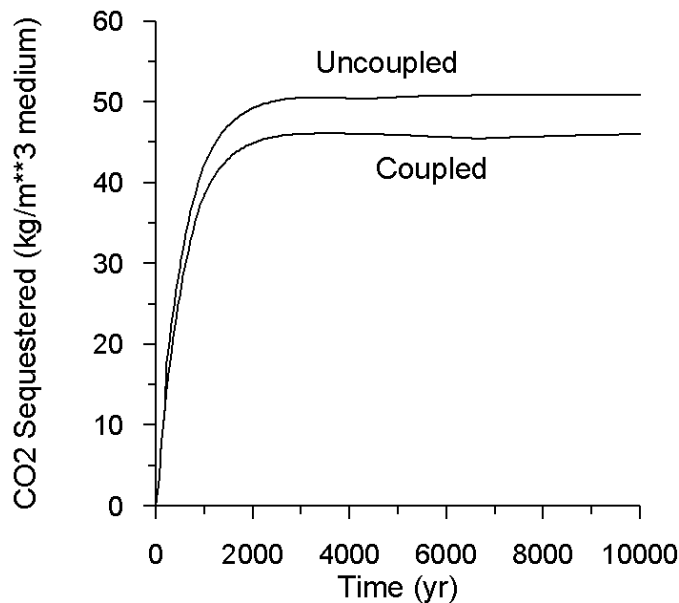


35

**Figure 19**. $CO_2$ sequestered over time by secondary carbonate minerals for uncoupled and coupled $CO_2$ gas phase transfer to the brine with gas phase depletion.

The modeled geochemical processes show that substantial changes in porosity can occur as a result of acid gas induced dissolution of matrix minerals, and the more distal precipitation of secondary carbonates. A small change in porosity of the injection zone host rock can result in a significant change in permeability, which can modify fluid flow. The present simulations monitor porosity changes only without corresponding corrections in permeability and modification to fluid flow. This feedback between flow and chemistry could be important in affecting injection pressure, and in modifying the distribution of geochemical reaction fronts and secondary mineral deposition.

In addition to model limitations relating to the hydrogeology, there exist several recognized geochemical limitations, which can be broadly subdivided into two categories: (1) those due to a lack of relevant thermochemical data and (2) those caused by insufficient kinetic data.

Incorporation of the thermodynamic properties of potential sulfate salt precipitates in the system was not undertaken for this study. A literature review indicates that several aluminum sulfates other than alunite that could also precipitate were sulfur dioxide to be co-injected with $CO_2$ and disproportionate into sulfuric acid and hydrogen sulfide (Bassett and Goodwin, 1949; Henry and Brooks King, 1949 and 1950; Nordstom, 1982). The cited studies did not evaluate the solubilities of aluminum sulfates incorporating alkali metal or other metal cations, of which several have been observed in nature. It is also probable that the initially precipitated phases would be metastable, depending on the degree of supersaturation and kinetic factors, as is discussed further below. Amorphous or poorly crystalline metastable secondary hydrated alumino-silicates that could compete with aluminum sulfates for aluminum, such as allophane or imogolite precursors (Bilinski et al., 1990) were also omitted from the model. Furthermore, no consideration was given to the potential formation of anionic clays containing interstitial carbonate anions, e.g., scarbroite ($Al_5(OH)_{13}CO_3.5H_2O$) (Brindley, 1980), or other synthetic aluminum hydroxocarbonate clay structures, which have not been observed in nature (Pakter and Panesar, 1987), and which, like dawsonite, might be stable under high

CO$_2$ partial pressures and moderately acid conditions. Two other aluminum hydroxocarbonates, occasionally associated with dawsonite occurrences, alumohydrocalcite (CaAl$_2$(CO$_3$)$_2$(OH)$_4$.3H$_2$O), and tunisite (NaCa$_2$Al$_4$(CO$_3$)$_4$(OH)$_8$Cl), were also omitted. Aqueous phase speciation is also incompletely described. Thus, evidence exists for the formation of aluminum carbonate complexes, Al$_2$(OH)$_2$CO$_3$$^{2+}$ and Al$_3$(OH)$_4$HCO$_3$$^{4+}$, (Hedlund et al., 1987), which could greatly enhance aluminum solubility and enhance aluminum transport, but were not incorporated, because of the substantial differences between the experimental conditions under which these complexes were characterized and those required for the model. Aluminum silicate species have also been identified (Pokrovski et al., 1998; Salvi et al., 1998; Swaddle, 2001), but were not included, as they are relatively weak, and unlikely to affect the principal findings of the paper.

The most substantial kinetic limitations of the current simulation concern the omission of rate equations describing the homogeneous disproportionation of SO$_2$ in the aqueous phase as given by Eq. 4. In the current model, disproportionation is assumed to be instantaneous, approximating conditions in which sulfuric acid generation is observed in magmatic hydrothermal systems as confirmed by laboratory experiments (Kusakabe et al., 2000). A search of the literature has yielded very little useful information that would allow for the quantitative modeling of this reaction. It is unlikely that experiments to define the rate of reaction would be easily accomplished, as reaction products with intermediate oxidation states are likely to form (Druschel et al., 2003). The reaction could also be catalyzed by transition metal cations, which would be present in any natural system (Kraft and Van Eldik, 1989). Ryabinina and Oshman (1972) investigated the thermal decomposition of aqueous H$_2$SO$_3$ at 120 - 140°C and found the reaction to be autocatalytic with an S$_2$O$_3$$^{2-}$ intermediate product. The activation energy for the reaction was 89 kJ/mol. Rempel et al. (1974) reported on the decomposition kinetics of 0.51 - 5.20 $M$ NaHSO$_3$ aqueous solutions in an autoclave at 110 - 180°C and with pH values between 2 and 5. The process was apparently autocatalytic with a (S$_2$O$_3$.SO$_2$)$^{2-}$ intermediate. An effective activation energy of 69 kJ/mol was reported. Khorunzhii et al. (1984) investigated the kinetics for disproportionation of sulfur dioxide in hydrochloric acid solutions, but no further information is given in the citation.

It is expected that the presence of dissolved sulfurous acid would lead to the precipitation of insoluble sulfite phases in the host aquifer. The two most important naturally occurring sulfites are hannebachite ($CaSO_3.0.5H_2O$) and orschallite ($Ca_3(SO_3)_2(SO_4).12H_2O$). $CaSO_3$ can substitute (as $CaSO_3.2H_2O$) into gypsum $CaSO_4.2H_2O$ and form a partial solid solution series (Setoyama and Takahashi, 1978, 1979; Takahashi and Setoyama, 1982). Similarly, $CaSO_4.0.5H_2O$ can substitute into the $CaSO_3.0.5H_2O$ structure up to a mol fraction of at least 0.12 (Jones et al., 1977a,b). Orschallite is also observed to form a partial solid solution series $Ca_3(SO_3)_x(SO_4)_{(3-x)}.12H_2O$, where $1 \leq x \leq 3$ (Zangen and Cohen, 1985; Cohen and Zangen, 1985). The cited authors conducted thermogravimetric analysis and differential scanning calorimetry on discrete members of the solid solution. Future studies concerning the subsurface co-disposal of $SO_2$ should incorporate appropriate kinetic and thermodynamic data pertaining to $SO_2$ and sulfite stability, and incorporation of the above-cited sulfite minerals. A direct consequence of kinetic control of $SO_2$ disproportionation is that $SO_2$ would partition between the compressed $CO_2$ fluid and the surrounding pore water. Mass transfer kinetics and local $SO_2$ thermodynamic equilibrium between the pore water and the injected $CO_2$ fluid would also require consideration.

Finally, a few words should be devoted to model limitations as they relate to nucleation, growth, and ripening of secondary minerals. Failure to account for such processes excludes from consideration the formation of metastable secondary phases in the system, and their eventual transformation into more stable phase assemblages as described by the Ostwald Rule of Stages (Ostwald, 1897). Earlier modeling of the Ostwald Rule is limited to those undertaken by Steefel and Van Cappellen (1990) and Ozkan and Ortoleva (2000). Substantial refinements would be needed to successfully model the systems under consideration in this paper. Of necessity, such modeling requires knowledge of the interfacial free energies of the participating phases, and quantification of the Gibbs free energy of heterogeneous nucleation under ambient subsurface conditions. Neither of these parameters is easy to obtain or quantify.

## 6. Model Comparisons

### 6.1. Earlier Modeling

The present model results are generally consistent with those by Knauss et al. (2005). The co-injection of $H_2S$, compared to injection $CO_2$ alone, does not significantly affect pH distribution and the mineral alteration pattern, whereas the co-injection of $SO_2$ results in a substantially different pH distribution and mineral alteration pattern. The formation of sulfate-bearing minerals such as anhydrite will change the reservoir porosity and permeability. Formation of dawsonite and silica phases (previous investigators used quartz as the silica phase) are also consistent. In the present study, we considered as additional secondary phases sulfur-bearing alunite and carbonate ankerite. Alunite precipitation follows $SO_2$ injection, whereas ankerite forms in all three acid-gas injection simulations. In the previous study, however, calcite precipitates in the $CO_2$ trapping zone (75 - 300 m distant from the injection well). In our studies, calcite does not precipitate in the $CO_2$ trapping zone, because we used a multiphase flow model, and a separate $CO_2$ phase remains during the simulation, keeping the pH low. Another difference is that our simulation time is much longer and gives a more detailed presentation of mineral alteration and acid-gas sequestration over time.

Batch geochemical modeling by Palandri and Kharaka (2005) shows that iron is transformed almost entirely to siderite or ankerite and sulfur is converted predominantly to dissolved sulfate. These findings are consistent with our simulations indicating dissolution of hematite and precipitation of siderite and ankerite. Anhydrite and alunite were not considered in the simulations of Palandri and Kharaka (2005).

Experimental work conducted by Kaszuba et al. (2005), who used a 5.5 molal NaCl brine–rock system at $200^{o}C$ and 200 bars with a duration of about 2.5 months, revealed the initial growth of magnetite and its later disappearance, followed by nucleation and growth of siderite. Their findings are consistent with our modeling. However, dawsonite was not observed in the experiments.

## 6.2. Field observations

Few mineralogical descriptions of the alteration of sandstone in the presence of high-pressure $CO_2$ are available in the literature that would allow comparison with the simulations presented in this paper. Those of interest usually reflect past accumulations of $CO_2$ associated with magmatic or volcanic activity. An example is given by Moore et al. (2005), who describe the formation of secondary dawsonite and kaolinite in siltstones of the Permian Supai Formation of the Springerville-St. John $CO_2$ field on the border between Arizona and New Mexico. They observed secondary dawsonite spatially associated with corroded plagioclase, which is consistent with our simulations. Furthermore, their determination that kaolinite formed subsequent to dawsonite deposition following a decline in the $CO_2$ pressure is consistent with our finding that kaolinite is unstable during the precipitation of dawsonite. In contrast, the Supai Formation appears to have been more oxidizing, with a limited capacity to provide $Fe^{2+}$ for the stabilization of ankerite. Moore et al. (2005) found very little dawsonite in samples from the Springerville-St. John $CO_2$ field, for which any number of explanations might be given: (1) the $CO_2$ partial pressure did not attain the level present in our simulations, (2) dawsonite crystallization may be kinetically hindered by the dissolution rate of Al-bearing precursor minerals or by low Al or low Na concentrations in the pore water, and (3) decarbonation could have followed $CO_2$ depressurization, as suggested by the late stage deposition of kaolinite.

Another recent paper (Watson et al., 2004) describes mineralogical and groundwater changes caused by magmatic carbon dioxide invading a gas reservoir in a lithic sandstone of the Pretty Hill Formation in the Ladbroke Grove gas field in South Australia. An important feature of this field example is that the mineralogy can be compared with an adjacent unmodified methane gas reservoir in the same formation. In contrast to the Supai Formation of Arizona and New Mexico, the conditions in this high-pressure $CO_2$ field are such that $Fe^{2+}$ is available for the stabilization of siderite and ankerite. In this respect, the Ladbroke Grove field more closely represents the conditions of our simulation. Field observations consistent with our simulation results include the destruction of chlorite in the lithic fragments and net corrosion of the feldspars, a

reduction in the concentration of calcite, an increase in the concentration of siderite, a significant increase in the quantity of ankerite, and a small increase in the quantity of quartz. However, no dawsonite was reported even though an evaluation of the coexisting groundwater indicates that it should have been supersaturated with respect to this mineral. A substantial increase in the concentration of kaolinite is observed, which is in conflict with our simulation. The differences, especially in relation to the stabilization of dawsonite, might be explained by the higher $CO_2$ pressure (i.e., 200 vs. approximately 150 bar) and the higher $Cl^-$ and $Na^+$ concentrations of the simulation.

The question of the occurrence or non-occurrence of dawsonite in the Springerville-St. John $CO_2$ or Ladbroke Grove fields suggests the need for further study of the nucleation, precipitation, and dissolution kinetics of dawsonite in relation to the principal components defining its stability field, $P_{CO2}$, NaOH, $Al_2O_3$, and temperature. The dawsonite stability field must also be constrained by associated paragenetic assemblages observed in the field. Furthermore, as noted elsewhere, the relative quantities of dawsonite and other carbonates that precipitate in a given reservoir depend also on the nature and magnitude of dissolution rates for precursor minerals. Thus, the discrepancy between field observations and model results may reflect the sensitivities of the investigated systems to uncertainties in rate constants of heterogeneous reactions kinetics.

Other field evidence suggests that magmatic $CO_2$ can also lead to the formation of dawsonite in arenaceous sedimentary formations, notably in the Bowen, Gunnedah, and Sydney Basins of New South Wales (Baker et al., 1995), and the Denison Trough of east-central Queensland (Baker, 1991; Baker and Caritat, 1992). Dawsonite and kaolinite in these sedimentary accumulations appear to have been produced at the expense of detrital feldspars, in general agreement with the observations of Moore et al. (2005). Note, however, that feldspar destruction is incomplete, and on occasion, dawsonite is found in juxtaposition with unaltered feldspar. The field evidence is therefore suggestive of slow feldspar corrosion rates if not the eventual stabilization of feldspars. In these sedimentary formations, the occurrence of dawsonite is unrelated to the preceding precipitation or dissolution of calcite, siderite, and ankerite, which is attributed to early diagenesis and subsequent organic maturation (Baker, 1991).

Carbonate paragenesis in sedimentary formations invaded by magmatic $CO_2$ can vary in degree and complexity. The mineralogy, burial history, diagenesis, organic maturation, temperature, and connate water salinity all play a role in addition to the timing and extent of magmatic $CO_2$ involvement. Thus, it is hardly surprising that agreement between the present simulations and field observations is not perfect in all respects.

## 7. Findings and Recommendations

We have developed a conceptual model for injection of $CO_2$ with $H_2S$ or $SO_2$ in a sandstone formation, using hydrogeologic properties and mineral compositions commonly encountered in U.S. Gulf Coast sediments. We have performed six simulations of acid-gas injection into a 1-D radial region of an arkosic formation surrounding an injection well, at 200 bar pressure and 75°C. Major findings are as follows:

(1)     The co-injection of $H_2S$, compared to injection $CO_2$ alone, does not significantly affect pH distribution, mineral alteration, or $CO_2$ mineral sequestration. The co-injection of $SO_2$ results in a substantially different pH distribution and mineral alteration.

(2)     A zonal distribution of mineral alteration and formation of secondary minerals is observed in the simulations, which reflects the composition of the injected gas and pH distribution. With co-injection of $SO_2$, a larger and more strongly acidified zone is obtained. Precipitation of secondary sulfates with a pyrite occurs within a pH range between 4 and 5, at radial distances ranging from 50 to 150 m. Precipitation of carbonates occurs in peripherally higher pH regions ($CO_2$ trapping zone) beyond the acidified zones.

(3)     For both $CO_2$ only and $CO_2$-$SO_2$ injections, the patterns and amounts of carbonate mineral precipitation in the $CO_2$ trapping zone are similar, although the acidified zone resulting from injection of $CO_2$ extends only to a radial distance of 50 m from the well bore, compared

with that resulting from the co-injection of $SO_2$, which extends to 200 m. $CO_2$ is sequestered primarily in ankerite and dawsonite, together with a small amount of siderite. After 10,000 years, $CO_2$ mineral trapping could reach about 40-50 kg per cubic meter of injection zone host rock, which is very close to the maximum possible for the specified host rock mineralogy.

(4)    The $CO_2$ trapping capability depends on the primary mineral composition. Precipitation of siderite and ankerite requires $Fe^{2+}$ supplied by the dissolution of iron-bearing minerals, such as chlorite $(Mg_{2.5}Fe_{2.5}Al_2Si_3O_{10}(OH)_8)$, and by reduction of $Fe^{3+}$ in small amounts of hematite. Precipitation of dawsonite requires $Na^+$ and $Al^{3+}$ provided by oligoclase $(Ca_{0.2}Na_{0.8}Al_{1.2}Si_{2.8}O_8)$ dissolution. Essentially no $Na^+$ is provided from sodium chloride in the brine. The initial abundance of chlorite and oligoclase therefore affects the $CO_2$ mineral-trapping capability.

(5)    Most injected $SO_2$ is ultimately trapped as sulfate by alunite precipitation, yielding a peak volume fraction of 7%, with additional contributions by anhydrite and as minimal sulfide in the form of pyrite. Pyrite also forms during co-injection of $CO_2$ and $H_2S$. Precipitation of the above cited minerals occurs primarily during the 100-year injection period, because the $H_2S$ or $SO_2$ inventory is small, and precursor mineral corrosion is very rapid under low pH conditions induced by sulfuric acid generation.

(6)    The injection of acid gases and the resulting mineral alteration leads to changes in porosity. Porosity increases significantly in the acidified zones where mineral dissolution dominates. With co-injection of $SO_2$, the porosity increases from an initial 0.3 to 0.43 after 100 years. However, within the $CO_2$ mineral-trapping zone, the porosity decreases to about 0.28 for both cases of $CO_2$ alone and $CO_2 + SO_2$, because of the precipitation of secondary carbonates in the rock matrix. The precipitation of secondary sulfates at the acidification

front causes the porosity to decrease to 0.23. The location of minimum porosity coincides with the maximum precipitation of alunite. A small change in porosity can result in a significant change in permeability, which could modify fluid flow.

(7)     The limited information currently available for the mineralogy of natural high-pressure $CO_2$ gas reservoirs is generally consistent with our simulation.

The simulations of acid gas injection presented in this paper are preliminary, as they are limited by model simplifications, and by insufficient thermodynamic, kinetic and physical data. Further refinements will be required, although the prioritizing extent and direction of such improvements will depend on future $CO_2$ sequestration programs. Thus, if future coal-burning power plants were to utilize IGCC technology, and co-injection of $H_2S$ with $CO_2$ is contemplated, significant added complexity over the disposal of $CO_2$ alone would not be expected, and modest refinements would be in order. For example, more realistic simulations would require modeling of the injection of a mixed $CO_2$-$H_2S$ gaseous phase, and differential partitioning of $H_2S$ and $CO_2$, during dissolution of the two gases in the aquifer pore water. In contrast, in the less likely event that volatile products of conventional combustion were to be co-injected with $CO_2$, the current model would need significant refinement. Current modeling predicts that the co-injection of $SO_2$ with $CO_2$ would lead to aggressive rock alteration of the injection zone in the vicinity of the well bore, due primarily to the formation of sulfuric acid and small amounts of $H_2S$ during $SO_2$ disproportionation. The model omits the kinetics of the $SO_2$ disproportionation, which if taken into account, would delay $SO_2$ decomposition and lead to the precipitation of secondary sulfite minerals.

Sensitivity studies show that arbitrary changes in rates of reaction, or the representation of more complex but more realistic mineral dissolution kinetics, can significantly modify the predicted stability fields of secondary alteration minerals. This finding clearly demonstrates that model validation using natural analogues of high-pressure $CO_2$ reservoirs will be meaningful only with further model refinement and

testing as proposed, and by a more accurate and comprehensive definition of field parameters to ensure model conformity.

**Acknowledgement**

**References**

Abercrombie, H.J., Hutcheon, I.E., Bloch, J.D., de Caritat, P. 1994. Silica activity and the smectite-illite reaction. Geology, 22, 539-542.

Apps, J.A., 2006. A review of hazardous chemical species associated with $CO_2$ capture from coal-fired power plants and their potential fate during $CO_2$ geologic storage. Lawrence Berkeley National Laboratory Report LBNL-59731, 60 pp.

Arnorsson, S., and Stefansson, A. 1999. "Assessment of feldspar solubility constants in water in the range 0° to 350°C at vapor saturation pressures." *American Journal of Science, 299*, (3), 173-209.

Bachu, S., Gunter, W.D., Perkins, E.H., 1994. Aquifer disposal of $CO_2$: hydrodynamic and mineral trapping. Energy Convers. Mgmt. 35, 269-279.

Bachu, S., 1996. Hydrogeological and numerical analysis of $CO_2$ disposal in deep aquifers in the Alberta Sedimentary Basin. Energy Convers. Mgmt. 37(6-8), 1167 - 1174.

Bachu, S., Haug, K, Michael, K., Buschkuehle, B.E., Adams, J. J., 2005. Deep injection of acid gas in Western Canada, Chapter 48 in Underground Injection Science and Technology (Chin-Fu Tsang and John A. Apps, Eds), p. 623-635. Developments in Water Sciences 52, Elsevier, Amsterdam, Holland.

Baker, J.C., 1991. Diagenesis and reservoir quality of the Aldebaran Sandstone, Denison Trough, east-central Queensland, Australia. Sedimentology 38, 819-838.

Baker, J.C., Caritat, P., 1992. Postdepositional history of the Permian Sequence in the Denison Trough, Eastern Australia. Am. Assoc. Petrol. Geol. Bull. 76(8), 1224-1249.

Baker, J.C., Bai, G.P., Golding, S.D., Keene, J.B., 1995. Continental-scale magmatic carbon dioxide seepage recorded by dawsonite in the Bowen-Gunnedah-Sydney Basin system, Eastern Australia. J. Sed. Res. A65(3), 522-530.

Bassett, H., Goodwin, T.H., 1949. The basic aluminum sulphates. J. Chem. Soc., 2239-2279.

Bilinski, H., Horvath, L., Ingri, N., Sjoeberg, S., 1990. Aluminosilicate phases during initial clay formation: Hydrogen ion-aluminum-oxalic acid-silicic acid-sodium system. J. Soil Sci, 41(1), 119-132.

Brindley, G.W., 1980. Scarbroite, $Al_5(OH)_{13}CO_3.5H_2O$, compared with gibbsite and hydrotalcite. Min. Mag., 43, 615-618.

Carroll, S.A., Knauss, K.G., 2005. Dependence of labradorite dissolution kinetics on $CO_2(aq)$, $Al(aq)$, and temperature. Chem. Geol. 217, 213-225.

Chai, L., and Navrotsky, A., 1996, Synthesis, characterization, and energetics of solid solution along the dolomite-ankerite join, and implications for the stability of ordered $CaFe(CO_3)_2$, Am. Mineral., 81, 1141-1147.

Cohen, A., Zangen, M. 1985. Studies on alkaline earth sulfites – VIII. Thermal behaviour of $Ca_3(SO_3)_2(SO_4).12H_2O$ and its solid solution in calcium sulfite tetrahydrate and crystallographic data on dehydrated salts. Rev. Chim. Min., 22, 427-436.

Corey, A. T., 1954, The interrelation between gas and oil relative permeabilities, Producers Monthly, 38 – 41.

Druschel, G.K., Hamers, R.J., Banfield, J.F. 2003. Kinetics and mechanism of polythionate oxidation to sulfate at low pH by $O_2$ and $Fe^{3+}$. Geochim. Cosmochim. Acta, 67(23), 4457-4469.

Effenberger, H., Kluger, F., Pertlik, F., Zemann, J., 1981. Tunisit: Kristallstruktur and Rvision der chemischen Formel. Tschermaks Min. Petr. Mitt., 28, 65-77.

Ennis-King, J., and Paterson, L., 2003. Role of convective mixing of the long-term storage of carbon dioxide in deep saline formations, Paper SPE 84344, Presented at Society of Petroleum Engineers Annual Fall Technical Conference and Exhibition, Denver, CO, October 2003.

Gunter W.D., Perkins, E.H., McCann, T.J., 1993. Aquifer disposal of $CO_2$-rich gases: Reaction design for added capacity. Energy Convers. Mgmt. 34, 941-948.

Gunter W.D., Bachu, S., Law, D.H.S., Marwaha, V., Drysdale, D.L., MacDonald, D.E., McCann, T.J., 1996. Technical and economic feasibility of $CO_2$ disposal in aquifers within the Alberta Sedimentary Basin, Canada. Energy Convers. Mgmt. 37, 1135-1142.

Gunter W.D., Wiwchar, B., Perkins, E.H., 1997. Aquifer disposal of $CO_2$-rich greenhouse gases: extension of the time scale of experiment for $CO_2$-sequestering reactions by geochemical modeling. Mineral. and Petrol. 59, 121-140.

Gunter, W.D., Perkins, E.H., Hutcheon, I., 2000. Aquifer disposal of acid gases: modelling of water–rock reactions for trapping of acid wastes. Applied Geochemistry 15, 1085-1095.

Hedlund, T., Sjoeberg, S., Oehman, L. O., 1987. Equilibrium and structural studies of silicon(IV) and aluminum(III) in aqueous solution. 15. A potentiometric study of speciation and equilibria in the aluminum(3+)-carbon dioxide(g)-hydroxide system. Acta Chem. Scand., Ser. A: Phys. Inorg. Chem., A41(4), 197-207.

Helgeson, H.C., Kirkham, D.H., Flowers, G.C., 1981. Theoretical prediction of the thermodynamic behavior of aqueous electrolytes at high pressures and temperatures: IV. Calculation of activity coefficients, osmotic coefficients, and apparent molal and standard and relative partial molal properties to 600 C and 5 kb. Am. J. Sci. 281, 1249–1516.

Hellmann, R., Tisserand, D., 2006. Dissolution kinetics as a function of the Gibbs free energy of reaction: An experimental study based on albite feldspar. Geochimica et Cosmochimica Acta, 70, 364-383.

Henry, J.L., Brooks King, G. 1949. The system aluminum sulfate-sulfuric acid-water at 60°. J. Amer. Chem. Soc., 71, 1142-1144.

Henry, J.L., Brooks King, G. 1950. Phase rule investigation of the system $Al_2O_3$-$SO_3$-$H_2O$ at 60°, basic region. J. Am. Chem. Soc., 72, 1282-1286.

Holland, T.J.B., and Powell, R., 1998, In internally consistent thermodynamic data set for phases of petrological interest. *Journal of Metamorphic Geology*, 16(3), 309-343.

Johnson, J.W., Oelkers, E.H., Helgeson, H.C., 1992. SUPCRT92: A software package for calculating the standard molal thermodynamic properties of minerals, gases, aqueous species, and reactions from 1 to 5000 bars and 0 to 1000 degrees C. Computers and Geosciences 18, 899–947.

Johnson, J.W., Nitao, J.J., Steefel, C.I., Knaus, K.G., 2001. Reactive transport modeling of geologic $CO_2$ sequestration in saline aquifers: The influence of intra-aquifer shales and the relative effectiveness of structural, solubility, and mineral trapping during prograde and retrograde sequestration, In proceedings: First National Conference on Carbon Sequestration. Washington, DC.

Jones, B.F., Philip, S., Meserole, F.B. 1977a. Experimental and theoretical studies of solid solution formation in lime and limestone sulfur dioxide scrubbers, Volume 1. Final report. Radian Corp., Austin, Texas, USA. U.S. NTIS, PB Rep., 75 pp.

Jones, B.F., Lowell, P.S. Meserole, F.B. 1977b. Experimental and theoretical studies of solid solution formation in lime and limestone sulfur dioxide scrubbers, Volume 1I. Appendices. Radian Corp., Austin, Texas, USA. U.S. NTIS, PB Rep., 75 pp.

Kastner, M. 1979. Silica polymorphs. p. 99-109. *In* R.G. Burns, (ed), Marine Minerals. Short Course Notes, 6. Mineral. Soc. Am., Washington, D.C.

Kastner, M., Keene, J.B., Gieskes, J.M. 1977. Diagenesis of siliceous oozes – I. Chemical controls on the rate of opal-A to opal-CT transformation – an experimental Study. Geochim. Cosmochim. Acta. 4, 1041-1059.

Kaszuba, J.P., Janecky, D.R. and Snow, M.G., 2003. Carbon dioxide reaction processes in a model brine aquifer at 200$^o$C and 200 bars: Implications for geologic sequestration of carbon. Applied Geochemistry, 18(7): 1065-1080.

Kaszuba, J.P., Janecky, D.R., Snow, M.G., 2005. Experiment evaluation of mixed fluid reactions between supercritical carbon dioxide and NaCl brine: Relevance to the integrity of a geologic carbon repository. Chem. Geol. 217, 277-293.

Kharaka, Y.K.,  Cole, D.R., Thordsen, J.J., Kakouros, E., Nance, H.S. 2006. Gas-water-rock interactions in sedimentary basins: $CO_2$ sequestration in the Frio Formation, Texas, USA. Journal of Geochemical Exploration, 89, 183-186.

Khorunzhii,  B.I., Volodin, N.I., Zakharov, Yu.D., Fateeva, V.P. 1984.  Kinetics of disproportionation of sulfur dioxide in hydrochloric acid solutions [in Russian]. Khimiya i Tekhnol. Monomerov, M., p. 25-30.  CA 103-221785.1984

Knauss, K.G., Johnson, J.W., Steefel, C.I., 2005. Evaluation of the impact of $CO_2$, co-contaminant gas, aqueous fluid, and reservoir rock interactions on the geologic sequestration of $CO_2$. Chem. Geol. 217, 339-350.

Korbol, R., Kaddour, A., 1995.  Sleipner vest $CO_2$ disposal - injection of removed $CO_2$ into the Utsira Formation. Energy Convers. Mgmt. 36 (6-9), 509-512.

Kraft, J., Van Eldik, R. 1989.  Kinetics and mechanism of iron(III)-catalyzed autoxidation of sulfur(IV) oxides in aqueous solution. 2.  Decomposition of transient iron(III)-sulfur(IV) complexes.  Inorg. Chem., 28(12), 2306-2312.

Kulik, D.A. and Aja, S.U.  1997.  "The hydrothermal stability of illite: Implications of empirical correlations and Gibbs energy minimization." *Proceedings of the Fifth International Symposium on Hydrothermal Reactions, Gatlinburg, Tennessee, July 20-24, 1997*.  Palmer, D.A. and Wesolowski, D.J., eds.  Pages 288-292.  Oak Ridge, Tennessee:  Oak Ridge National Laboratory.

Kusakabe. M., Komoda, Y., Takano, B., Abiko, T., 2000. Sulfur isotopic effects in the disproportionation reaction of sulfur dioxide in hydrothermal fluids: implications for the $\delta^{34}S$ variations of dissolved bisulfate and elemental sulfur from active crater lakes. Journal of Volcanology and Geothermal Research 97, 287-307.

Lasaga, A.C., 1995. Fundamental approaches in describing mineral dissolution and precipitation rates. In: White, A.F., Brantley, S.L. (Eds.), Chemical Weathering Rates of Silicates Minerals, Reviews in Mineralogy, vol. 31. BookCrafters, Chelsea, MI, pp. 23–86.

Lasaga, A.C., 1998.  Kinetic Theory in the Earth Sciences.  Princeton University Press, Princeton, New Jersey.  811 p.

Lasaga, A.C., and A. Luttge. 2001. Variation of crystal dissolution rate based on a dissolution stepwave model.  Science (Washington, DC) 291, 2400-2404.

Lasaga, A.C. and Luttge, A.. 2003. A model for crystal dissolution. Eur. J. Mineral. 15, 603-615.

Lasaga, A.C., Soler, J.M., Ganor, J., Burch, T.E., Nagy, K.L., 1994. Chemical weathering rate laws and global geochemical cycles. Geochimica et Cosmochimica Acta, 58, 2361-2386.

Lohuis, J.A.O., 1993. Carbon dioxide disposal and sustainable development in The Netherlands, Energy Convers. Mgmt. 34(9-11), 815-821.

McPherson, B.J.O.L., Lichtner, P.C., 2001. $CO_2$ sequestration in deep aquifers, In proceedings: First National Conference on Carbon Sequestration. Washington, DC.

Moore, J., Adams, M., Allis, R., Lutz, S., Rauzi, S., 2005. Mineralogical and geochemical consequences of the long-term presence of $CO_2$ in natural reservoirs: An example from the Springerville–St. Johns Field, Arizona, and New Mexico, U.S.A. *Chemical Geology*, 217, 365-385.

Narasimhan, T.N., Witherspoon, P.A., 1976. An integrated finite difference method for analyzing fluid flow in porous media, Water Resour. Res. 12, 57–64.

Nordstrom, D.K. 1982. The effect of sulfate on aluminum concentrations in natural waters: some stability relations in the system $Al_2O_3$-$SO_3$-$H_2O$ at 298 K. Geochim. Cosmochim. Acta 46, 681-692.

Nsakala, N.Y., Marion, J., Bozzuto, C., Liljedahl, G., Palkes, M., Vogel, D., Gupta, J.C., Guha, M., Johnson, H., and Plasynski, S. 2001. *Engineering Feasibility of $CO_2$ Capture on an Existing US Coal-Fired Power Plant* . First National Conference on Carbon Sequestration, Washington, D.C.

Oelkers, E. H., Pokrovsky, O., Schott, J., 2002. An experimental study of magnesite dissolution and precipitation rates, 2002 Geological Society of America, Session 135 (1), October 27-30, Denver, Colorado.

Ostwald, W. 1897. Studien über die Bildung und Umwandlung fester Körper: Z. Phys. Chem. 22:289–330.

Ozkan, G., Ortoleva, P., 2000. A mesoscopic model of nucleation and Ostwald ripening/stepping. Application to the silica polymorph system. J. Chem. Phys. 112(23):10510-10525.

Palandri, J., Kharaka, Y.K., 2004. A compilation of rate parameters of water-mineral interaction kinetics for application to geochemical modeling. US Geol. Surv. Open File Report 2004-1068, 64 pp.

Palandri, J.L., Kharaka, Y.K., 2005. Ferric iron-bearing sediments as a mineral trap for $CO_2$ sequestration: Iron reduction using sulfur-bearing waste gas. Chem. Geol. 217, 351-364.

Packter, A., Panesar, K.S., 1987. The precipitation of aluminium hydroxocarbonates powders from aqueous solution: Precipitate compositions and precipitation mechanisms. Cryst. Res. Technol. 22(8), 1015-1022.

Parker, V.B. and Khodakovskii, I.L., 1995. Thermodynamic properties of the aqueous ions (II and III) of iron and key compounds of iron. J. Phys. Chem. Ref. Data, v. 24(5), p. 1699-1745.

Parkhurst, D. L., Thorstenson, D. C., and Plummer, L. N., 1980. PHREEQE: A computer program for geochemical calculations. US Geol. Surv. Water Resour. Invest. 80-96, 174 pp.

Pearce, J.M., Holloway, S., Wacker, H., Nelis, M.K., Rochelle, C., Bateman, K., 1996. Natural occurrences as analogues for the geological disposal of carbon dioxide. Energy Convers. Mgmt. 37 (6-8), 1123-1128.

Perkins, E.H., Gunter, W.D., 1995. A users manual for PATHARC.94: a reaction path-mass transfer program, Alberta Research Council Report ENVTR 95-11, 179 pp., Canada.

Perkins, E. H., Gunter, W.D., Hutcheon, I., Shevalier, M., Durocher, K., Emberley, S., 2002. Geochemical modelling and monitoring of $CO_2$ storage at the Weyburn site, Saskatchewan, Canada, 2002 Geological Society of America Annual Meeting, Session 174 (11), October 27-30, Denver, Colorado.

Pokrovski, G.S., Schott, J., Salvi, S., Gout, R., Kubicki, J.D., 1998. Structure and stability of aluminum-silica complexes in neutral to basic solutions. Experimental study and molecular orbital calculations. Min. Mag., 62A(Pt. 2), 1194-1195.

Pokrovsky, O.S., Golubev, S.V., Schott, J., 2005. Dissolution kinetics of calcite, dolomite, and magnesite at 15 $^{o}$C and 0 to 50 atm $pCO_2$. Chem. Geol. 217, 239-255.

Preis, W., and Gamsjager, H., 2002. Critical evaluation of solubility data: enthalpy of

formation of siderite. Phys. Chem. Chem. Phys. 4, 4014-4019.

Pruess, K., Xu, T., Apps, J., García, J., 2003. Numerical modeling of aquifer disposal of $CO_2$. SPE (Society of Petroleum Engineers) Journal, p. 49-59, March (2003).

Pruess, K., 2004. The TOUGH Codes - A family of simulation tools for multiphase flow and transport processes in permeable media. Vadose Zone Journal 3, 738-746.

Reed, M.H., 1982. Calculation of multicomponent chemical equilibria and reaction processes in systems involving minerals, gases and aqueous phase. Geochim. Cosmochim. Acta 46, 513-528.

Rempel, S.I., Ryabinina, A.F., Oshman, V.A. 1974. Kinetics and mechanism of the thermal decomposition of solutions of sulfur dioxide and bisulfites [in Russian]. Ural. Lesotekh. Inst., Sverdovsk. Deposited document, 31 p. CA 86-128024.

Rimstidt, J.D., 1997. Quartz solubility at low temperatures. Geochim. et Cosmochim. Acta 61, 2553-2558.

Rochelle, C.A., Bateman, K., Pearce, J.M., 1996. Fluid-rock interactions resulting from the underground disposal of carbon dioxide, In Bottrell, S. H. (ed.), Proc., 4th lnt. Symp. Geochem, Earth's Surf.. University of Leeds, Dep. of Earth Sciences, Leeds, UK., 448-452.

Rock, P.A., Mandell, G.K., Casey, W.H. and Walling, E.M., 2001. Gibbs energy of formation of dolomite from electrochemical cell measurements and theoretical calculations. Am. J. Sci. 301, 103-111.

Rosenbauer, R.J., Koksalan, T., Palandri, J.L., 2005. Experimental investigation of $CO_2$–brine–rock interactions at elevated temperature and pressure: Implications for $CO_2$ sequestration in deep-saline aquifers. Fuel Processing Technology 86, 1581-1597.

Ryabinina, A.F., Oshman, V.A. 1972. Thermal decomposition of aqueous sulfur dioxide solutions. Tr. Ural. Lesotekh. Inst., No. 28, 182-189 [in Russian]. CA 79:58115.

Salvi, S., Pokrovski, G.S., Schott, J., 1998. Experimental investigation of aluminum-silica aqueous complexing at 300°C. Chem. Geol., 151(1-4), 51-67.

Setoyama, K., Takahashi, S. 1978. Solid solution of calcium sulfate dihydrate and sulfite hemihydrate [In Japanese]. Yogyo Kyokaishi, 86(5), 133-137.

Setoyama, K., Takahashi, S. 1979. Solid solution of calcium sulfate dihydrate and sulfite hemihydrate. Part 2. [In Japanese]. Sekko to Sekkai, 161, 244-250.

Siffert, B., Wey, R. 1967. Quantitative study of the transformation of amorphous silicon into quartz between 230.deg. and 350.deg. in the presence of alkaline base. Silicates Industriels 32(12), 415-22.

Sonnenthal E., Ito, A., Spycher, N., Yui, M., Apps, J., Sugita, Y., Conrad, M., Kawakami, S., 2005, Approaches to modeling coupled thermal, hydrological, and chemical processes in the Drift Scale Heater Test at Yucca Mountain. *International Journal of Rock Mechanics and Mining Sciences*, 42, 6987-719.

Soong, Y., Goodman, A.L., McCarthy-Jones, J.R., Baltrus, J.P., 2004. Experimental and simulation studies on mineral trapping of $CO_2$ with brine. Energy Conversion and Management 45, 1845-1859.

Spycher, N., Pruess, K.,2005. $CO_2$-$H_2O$ mixtures in the geological sequestration of CO2: II. Partitioning in chloride brines at 12–100°C and up to 600 bar. Geochimica et Cosmochimica Acta, 69, 3309-3320.

Steefel, C.I., van Cappellen, P., 1990. A new kinetic approach to modeling water-rock interaction: The role of nucleation, precursors and Ostwald ripening. Geochim. Cosmochim. Acta 54, 2657-2677.

Steefel, C.I., Lasaga, A.C., 1994. A coupled model for transport of multiple chemical species and kinetic precipitation/dissolution reactions with applications to reactive flow in single phase hydrothermal system. Am. J. Sci. 294, 529-592.

Swaddle, T.W., 2001. Silicate complexes of aluminum(III) in aqueous systems. Coordination Chem. Rev., 219-221, 665-686.

Takahashi, S., Setoyama, K. 1982. Solid solution of calcium sulfate dihydrate and sulfite hemihydrate. 3. Effect of pH and metal ions on the formation of the solid solution of calcium sulfate dihydrate and sulfite hemihydrate [In Japanese]. Gypsum & Lime, 181, 290-294.

Treviño Coca, M. 2003. *Integrated Gasification Combined Cycle Technology*: IGCC. ELCOGAS, S.A., Club Español de la Energia. 95 p.

U.S. EPA, 2001. Code of Federal Regulations, Title 40- Protection of Environment, [Page 610-677], Chapter I--Environmental Protection Agency (Continued), Part 144--Underground Injection Control Program Subpart A--General Provisions, Sec. 144.3 Definitions [Revised as of July 1, 2001]. U.S. Government Printing Office.

Van Cappellen, P., Qui, L. 1997. Biogenic silica dissolution in sediments of the Southern Ocean. I Solubility. Deep Sea Research II, 44(5), 1109-1128.

Van Genuchten, M. Th., 1980. A Closed-form equation for predicting the hydraulic conductivity of unsaturated soils. Soil Sci. Soc. Am. J. 44, 892 – 898.

Verma, A., and Pruess, K., 1998. Thermohydrological conditions and silica redistribution near high-level nuclear wastes emplaced in saturated geological formations. *J. Geophys. Res*. 93, 1159-1173.

Watson, M.N., Zwingmann, N., Lemon, N.M., 2004. The Ladbroke Grove–Katnook carbon dioxide natural laboratory: A recent $CO_2$ accumulation in a lithic sandstone reservoir. *Energy*, 29(9-10), 1457-1466.

Weir, G.J., White, S.P., and Kissling, W.M., 1995. Reservoir storage and containment of greenhouse gases, in: K. Pruess (ed.), *Proceedings of the TOUGH Workshop '95*, Lawrence Berkeley National Laboratory Report LBL-37200, p. 233-238, Berkeley, California.

White, S.P., Allis, R.G., Moore, J., Chidsey, T., Morgan, C., Gwynn, W., Adams, M., 2005. Simulation of reactive transport of injected $CO_2$ on the Colorado Plateau, Utah, USA. Chem. Geol. 217, 387-405.

White, A.F., Peterson, M.L., 1990. Role of reactive surface area characterization in geochemical models. Chemical modeling of aqueous systems II. In: Melchior, D.C., Bassett, R.L. (Eds.). Am. Chem. Soc. Symp. Ser. 416, 416–475.

Wolery, T.J., 1992. EQ3/6: Software package for geochemical modeling of aqueous systems: Package overview and installation guide (version 7.0). Lawrence Livermore National Laboratory Report UCRL-MA-210662 PT I, Livermore, California.

Xu, T., Pruess, K., 2001. Modeling multiphase non-isothermal fluid flow and reactive geochemical transport in variably saturated fractured rocks: 1. Methodology. Am. J. Sci., 301, 16-33.

Xu, T, Apps, J.A., Pruess, K., 2003. Reactive geochemical transport simulation to study mineral trapping for $CO_2$ disposal in deep arenaceous formations, Journal of Geophysical Research 109, B05209, doi:10.1029/2003JB002792.

Xu, T, Apps, J.A., Pruess, K., 2004. Numerical simulation to study mineral trapping for $CO_2$ disposal in deep aquifers, Applied Geochemistry, 19, 917-936.

Xu, T, Apps, J.A., Pruess, K., 2005. Mineral sequestration of carbon dioxide in a sandstone-shale system. Chem. Geol. 217, 295-318.

Xu, T., E.L. Sonnenthal, N. Spycher, and K. Pruess, 2006. TOURGHREACT: A simulation program for non-isothermal multiphase reactive geochemical transport in variably saturated geologic media. Computer & Geosciences 32, 145-165, DOI information: 10.1016/j.cageo.2005.06.014.

Yeh, G.T., Tripathi, V.S., 1991. A model for simulating transport of reactive multispecies components: model development and demonstration. Water Resour. Res. 27, 3075-3094.

Zangen, M., Cohen, A. 1985. Studies on alkaline earth sulfites – VI. Thermal dehydration of $Ca(SO_3)_x(SO_4)_{1-x}.4H2O$. Thermochim. Acta, 85, 107-110.

Zerai , B., Saylor, B.Z., Matiso, G., 2006. Computer simulation of $CO_2$ trapped through mineral precipitation in the Rose Run Sandstone, Ohio. Applied Geochemistry, 21, 223-240.

**Appendix A. Dissolution of Primary Minerals during Injection of Acid Gases**

Figure A-1 shows water saturations along the radial distance (gas $CO_2$ saturations $S_g$ are complementary to water saturations, or $S_g = 1- S_l$). The fluid flow pattern obtained from all simulations is similar. Figures A-2 to A-4 illustrate the dissolution behavior of those primary minerals not included for discussion in the text. A careful scrutiny of these figures helps provide answers to questions relating to mineral alteration at elevated $CO_2$ partial pressures.
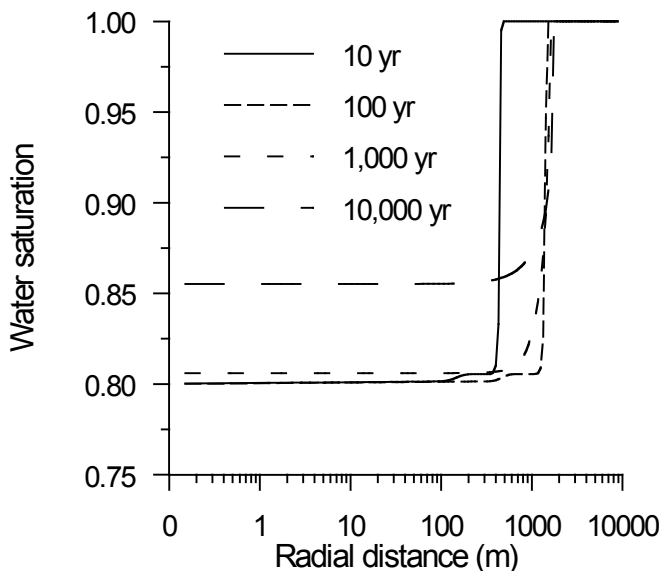


**Figure A-1**. Water saturations along radial distance at different times.
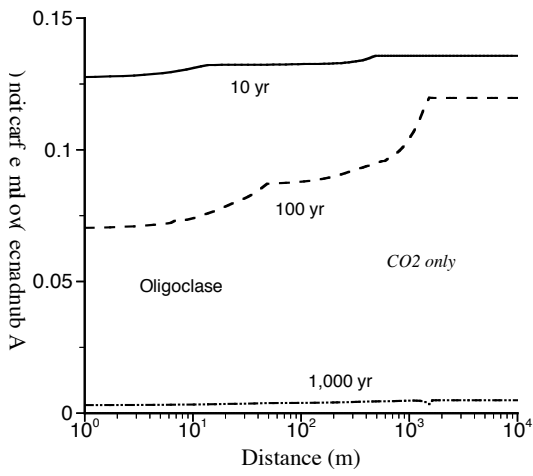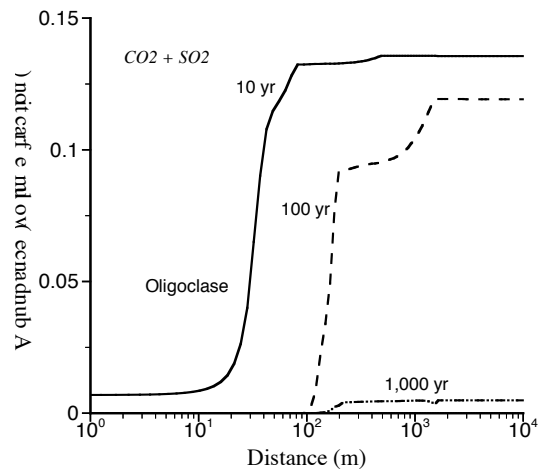
**Figure A-2**. Variation of oligoclase abundance with time.
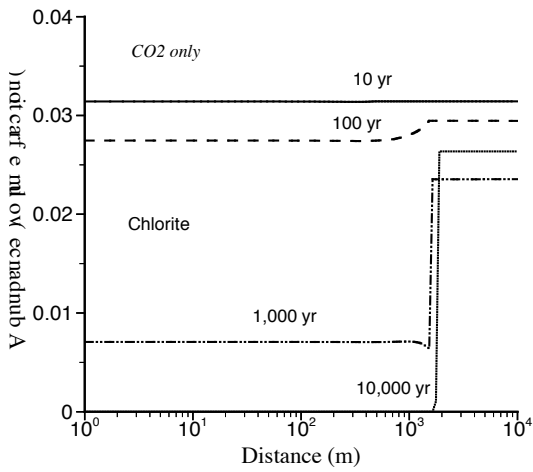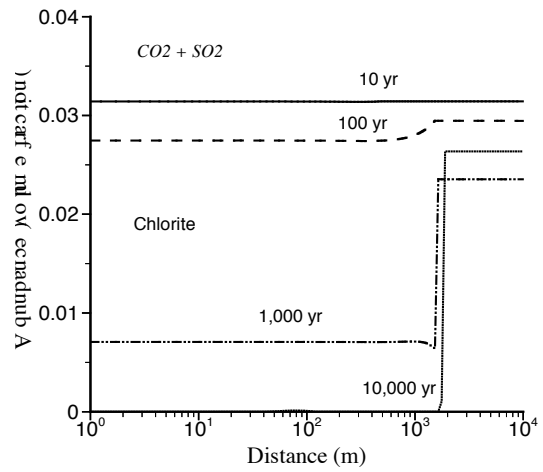


**Figure A-3**. Variation of chlorite abundance with time.
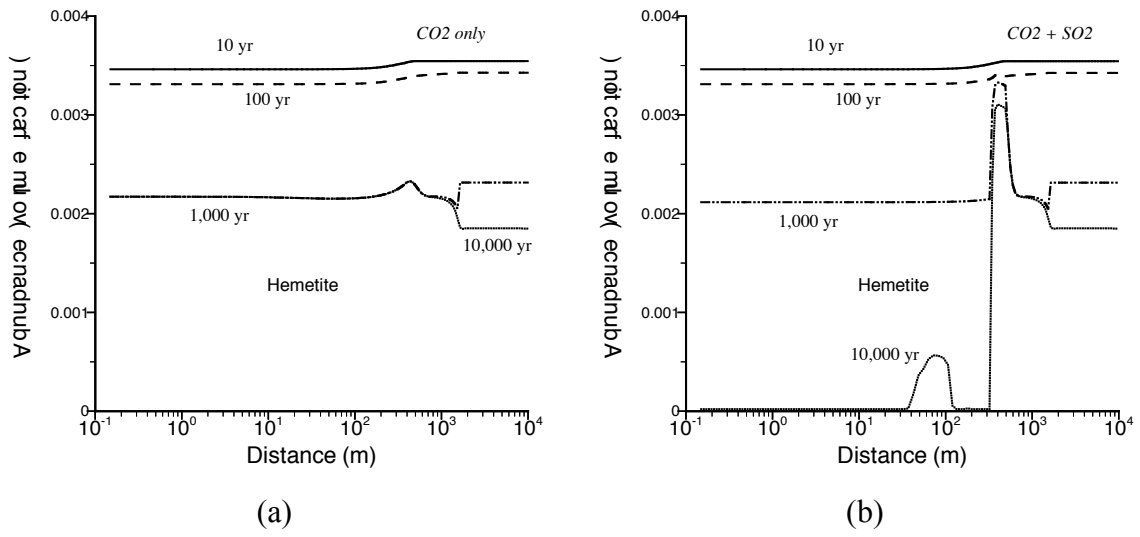
**Figure A-4**. Variation of hematite abundance with time.

# Appendix B. Additional Sensitivity Results

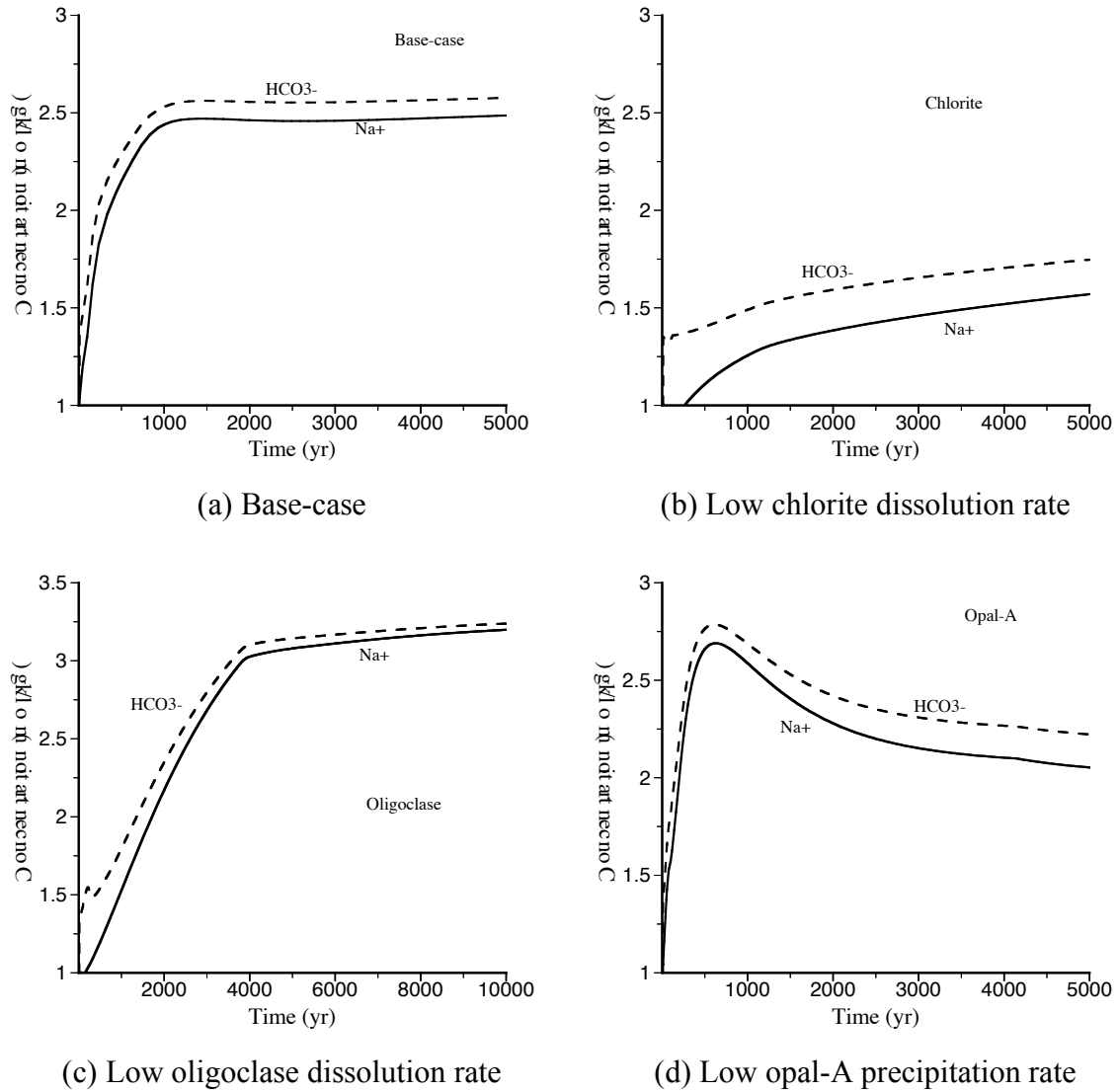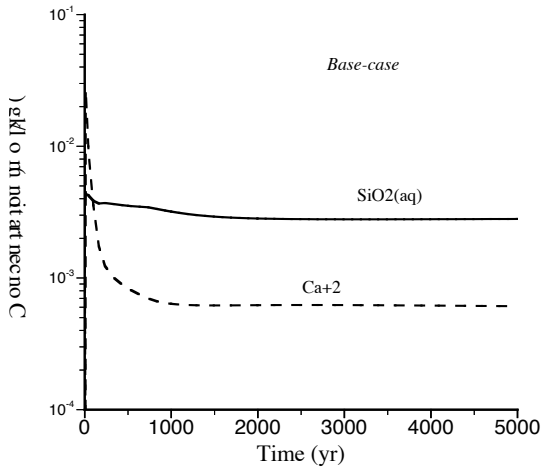Figures B-1 to A-4 give more results for sensitivity simulations not included for discussion in the text.



(a) Base-case

(b) Low chlorite dissolution rate

(c) Low oligoclase dissolution rate

(d) Low opal-A precipitation rate

**Figure B-1**. Evolution of aqueous concentrations of $Na^+$ and dissolved carbon (mainly $HCO_3^-$) for sensitivity simulations at 500 m distant from the borehole.
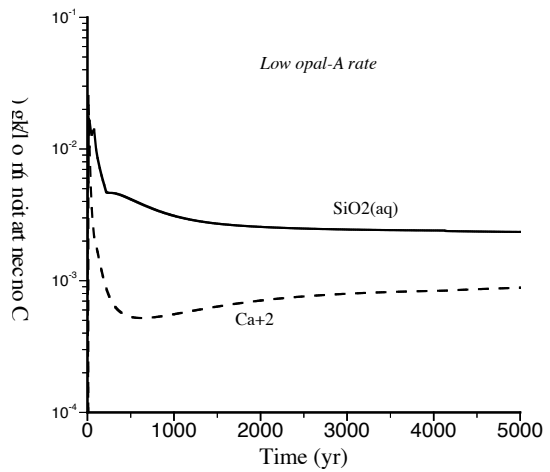
(a) Base-case
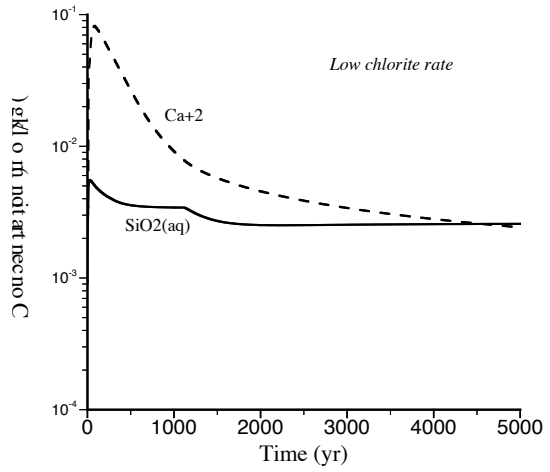
(b) Low chlorite dissolution rate
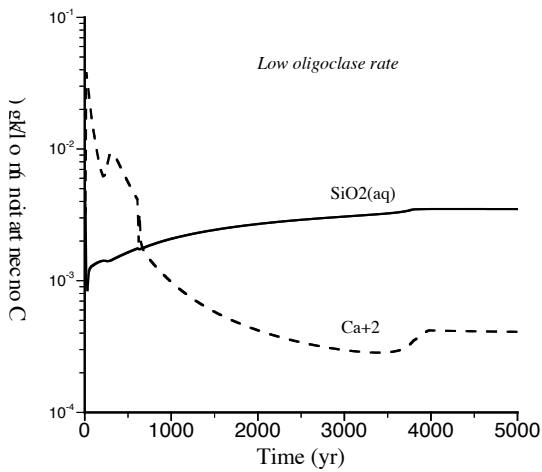
(c) Low oligoclase dissolution rate

(d) Low opal-A precipitation rate

**Figure B-2**. Evolution of aqueous concentrations of $Ca^{2+}$ and $SiO_2(aq)$ for sensitivity simulations at 500 m distant from the borehole.